ISTITUTO NAZIONALE DI FISICA NUCLEARE

Sezione di Milano

INFN/TC-88/16
28 aprile 1988

E. Acerbi and L. Rossi:

MECHANICAL THERMAL AND ELECTRICAL MEASUREMENTS ON MATERIALS AND COMPONENTS OF THE MAIN COILS OF THE MILAN SUPERCONDUCTING CYCLOTRON.

Servizio Documentazione
dei Laboratori Nazionali di Frascati

INFN - ISTITUTO NAZIONALE DI FISICA NUCLEARE
Sezione di Milano

INFN/TC-88/16
28 Aprile 1988

MECHANICAL THERMAL AND ELECTRICAL MEASUREMENTS ON MATERIALS AND COMPONENTS OF THE MAIN COILS OF THE MILAN SUPERCONDUCTING CYCLOTRON

E. Acerbi and L. Rossi

Universita' di Milano - Dipartimento di Fisica
INFN - Sezione di Milano

Abstract

The coils of the Milan Superconducting Cyclotron are the largest superconducting device built up to now in Italy and constitute the first superconducting magnet for accelerator in Europe. Because of the large stored energy (more than 40 MJ), of the high stresses and of the need of reliability, a lot of measurements were carried out as well on materials used for the coils, both on superconducting cable and structural materials, as on the main components of the coils and on two double pancakes prototypes (wound with full copper cable). In this paper the results on these measurements are reported and the results of tests on the prototypes are discussed. The aim is to provide an easy source of data for superconducting coils useful to verify calculations or to improve the performances.

INTRODUCTION

The Milan Superconducting Cyclotron [1,2,3], started to be built since the spring of 1981, is an high magnetic field accelerator for nuclear physics intended for ions from alpha to uranium; its foreseen performance ranges from 100 MeV/nucleon for the lightest, fully stripped, ions to 20 Mev/nucleon for the heaviest ions.
Because of multi-ions and variable energy characteristics, the magnetic field ranges from 2.2 T to 4.8 T, at the center of the machine, and it has to be largely varied in the radial profile to fit the isochronism requirements.
For the required induction level, superconducting coils (splitted in the median plane for beam injection and extraction) are needed. For the isochronism requirements both coils, the one over and the one under the median plane, are splitted in two parts, independently supplied, which may be oppositely excited.
The high field, over than 5 T (with the iron contribution which is approximately constant at 1.6 T), the large stored energy, more than 40 MJ, and the unusual forces and stresses that arise because of iron jacket and above all because of the opposite excitation of the coils, advice great care in the design and construction of the coils.
Moreover, because this is the first superconducting magnet designed and built in our laboratory, several tests on materials were carried out and some models and prototypes were built such as the model of the coils axial prestressing system and two prototypes of the double pancakes, wound by full copper cable.
To make easy the finding of the data hereby reported, we give the topics content:

I - CHARACTERISTICS OF THE SUPERCONDUCTING COILS

A detailed description of the superconducting coils and of the cryostat is given in [4], so hereby we only recall some characteristics useful for the present report.

The coils are wound with the double pancake technique and are in a liquid helium bath at nearly atmospheric pressure (T=4.3 K). The main charateristics of the coils and of the superconducting cable are summarized in table I and table II.

The cable is a grooved copper matrix in which the superconducting filamentary composite of Cu-NbTi is soft soldered (by using lead-tin alloy, 225 C of melting point).

Turn to turn (i.e. in the radial direction) insulation is assured by a mylar ribbon (11x0.15 mm^2) on which are glued mylar strips (11x0.35 mm^2) 4 mm wide and 5 mm spaced. Layer to layer (i.e. in the axial direction) insulation is obtained by using epoxy fiberglass composite strips (G11, 180 mm of radial length, 22 mm of average azimuthal width and 24 mm spaced, 1 mm of thickness).

The superconducting cable, wound on a 200 mm thick mandrel, was tensioned at 35 MPa and between the last eight turns a 150 MPa tensioned stainless steel tape (12x1.5 mm2) was inserted to lower the electromagnetic stress in the coils. The conductor ends are locked by means of stainless steel U-shaped clamps.

In the fig. 1 a sketch of the pancake structure is shown.

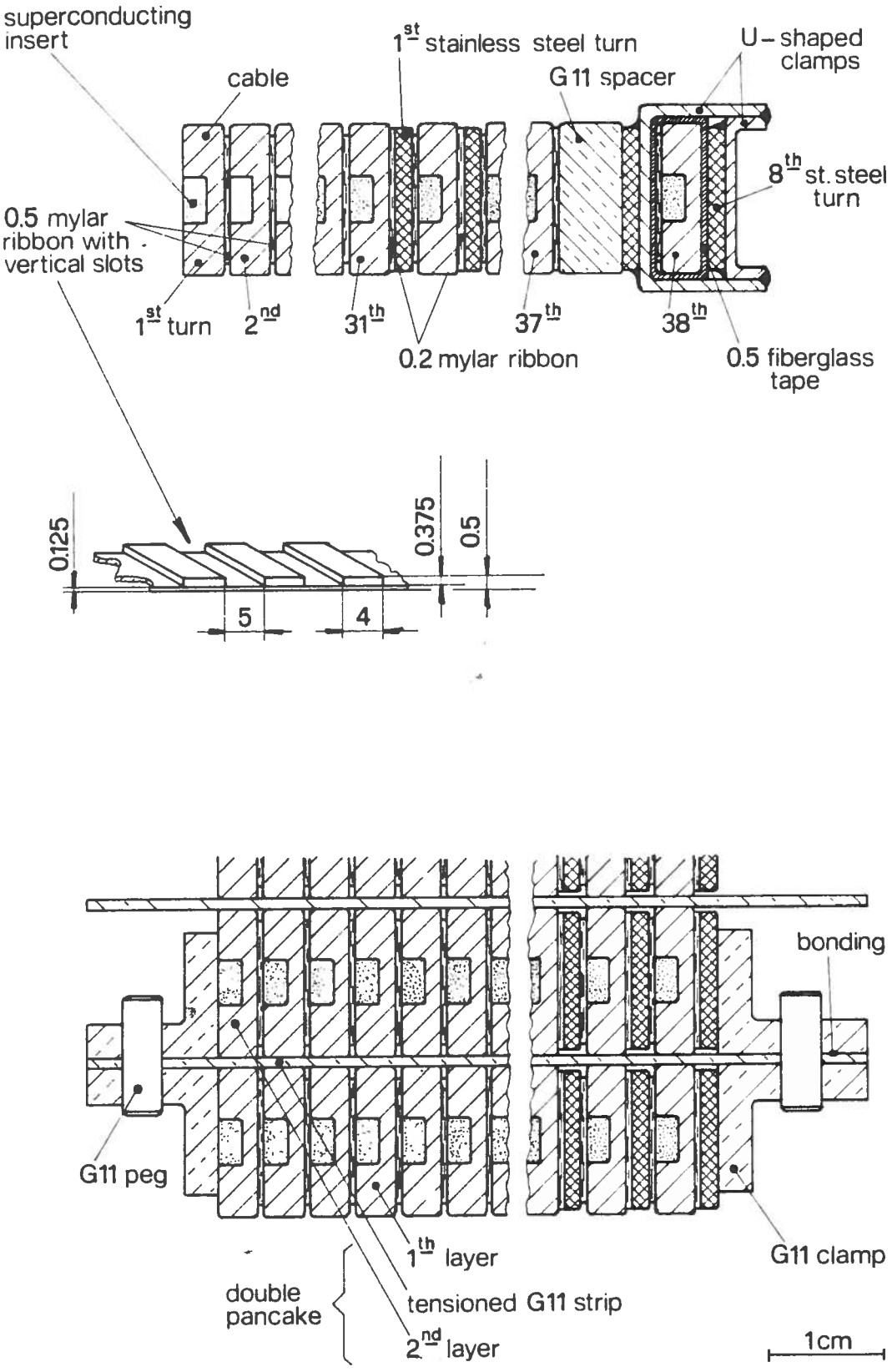

Fig.1 - Sketch of the superconducting cable and of the double pancake structure.

TABLE I - Coils parameters

internal radius (Room Temp.)	1000 mm
external radius (R.T.)	1165 mm
height (R.T.)	2x679 mm
midplane gap (R.T.)	120 mm
double pancakes	2x22
turns/double pancakes	2x38
turn to turn insulation	0.5 mm (mylar)
layer to layer insulation	1 mm (G11)
st. steel tape for banding	8 turnsx1.5 mm (AISI 316 L)
maximum nominal current	1960 A
maximum current density (overall)	3500 A/cm2
Maximum MMF	6.55 106 At
Inductance (without iron)	19.8 H
Stored energy	40 MJ
total cable length	22640 m
coil weight	9700 kg

TABLE II - Superconducting cable * characteristics

monolithic insert(Cu-NbTi 46%w)	3.6x1.8 mm^2
matrix (ETP copper, RRR=140)	13x3.5 mm^2
overall Cu/sc	20:1
twisting pitch	50 mm
filaments diameter	75 μm
filaments number	540
copper cold work	2 %
copper yield strength(0.2%)	120 MPa

* supplied by La Metalli Industriali (LMI), Florence - I

The coils, whose vertical section of the one above the median plane is shown in fig.2, are splitted in two parts, in the following named α and β sections, with independent power supplies; this is due to the necessity to have different field level and to fit as close as possible the different field shape needed for cyclotron isochronism. Moreover the β sections can be excited negatively (respect to the main field), so that they are pushed away from the median plane by about a 6 MN force. In order to compensate this force and avoid displacements, the coils are axially compressed (7 MN at room temperature) by means of beryllium copper rods (CuBe 2%, 2x144 inside rods with ϕ=10 mm and 2x72 outside rods with ϕ=14 mm). This CuBe tie rods are prestressed at about 300 MPa and coils prestressing is obtained by a stainless steel (AISI 316 L) plate.

When the coils are both positive supplied, this 7 MN force is added to the usual attractive force towards the median plane, so the total maximum compressive force is about 22 MN; this gives an axial

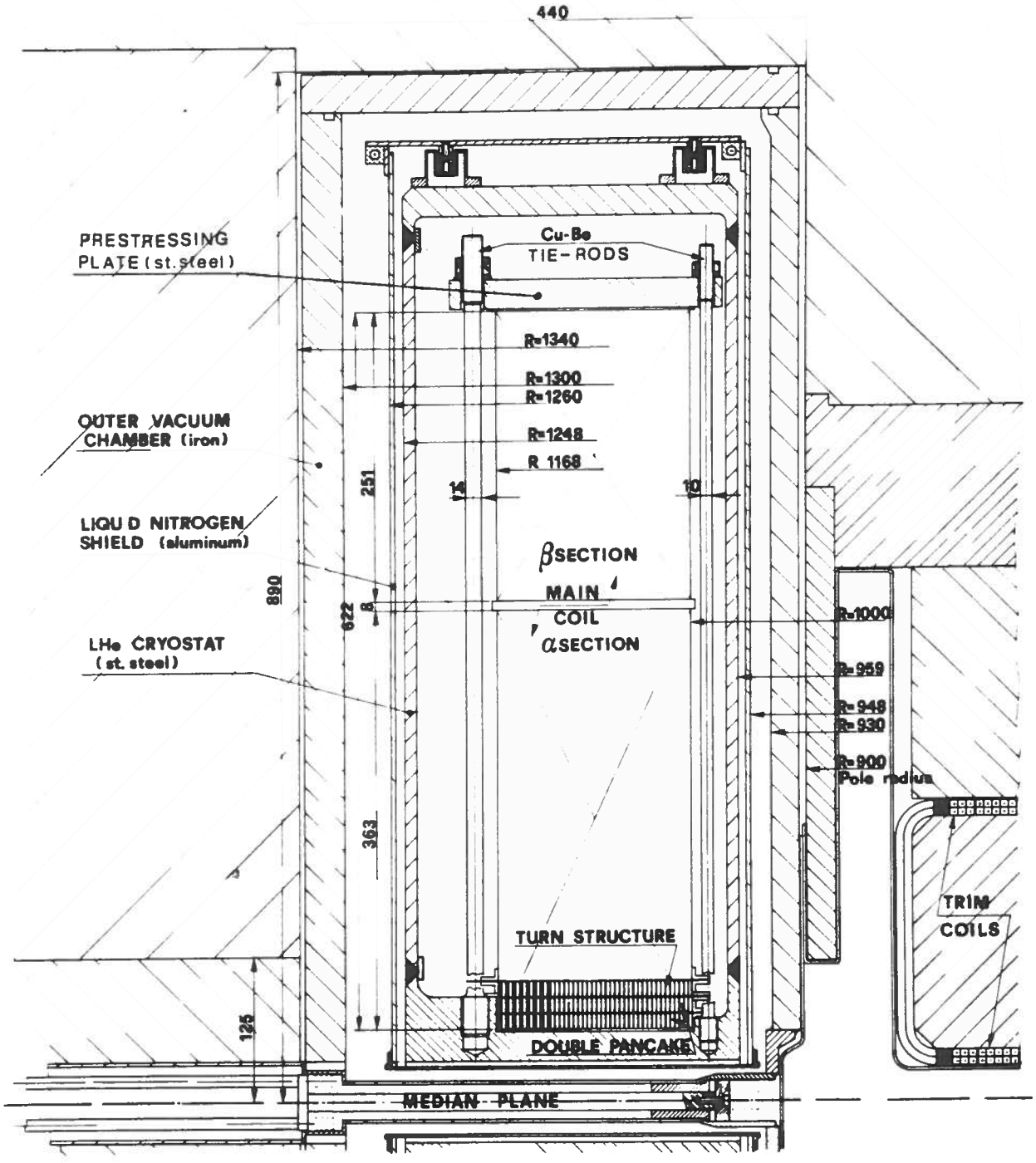

Fig.2 - Vertical section of the superconducting coils.

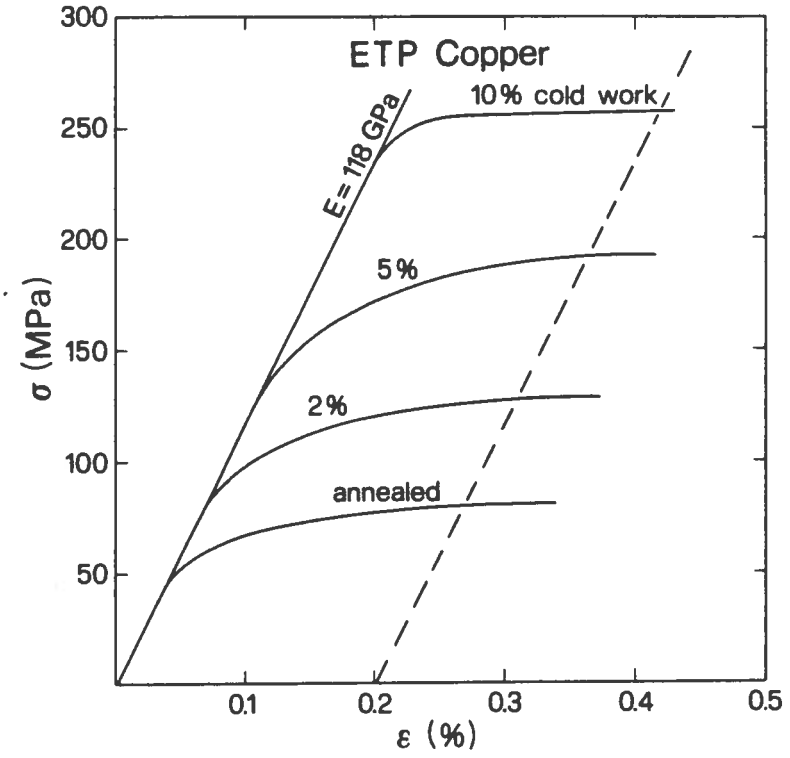

Fig.3 - The stress-strain diagram for the copper used for the matrix of the superconducting cable measured at different cold work percentage. Copper, ETP type, was supplied by LMI; measurements were carried out at room temperature. 2 % cold work grade was chosen for the cable.

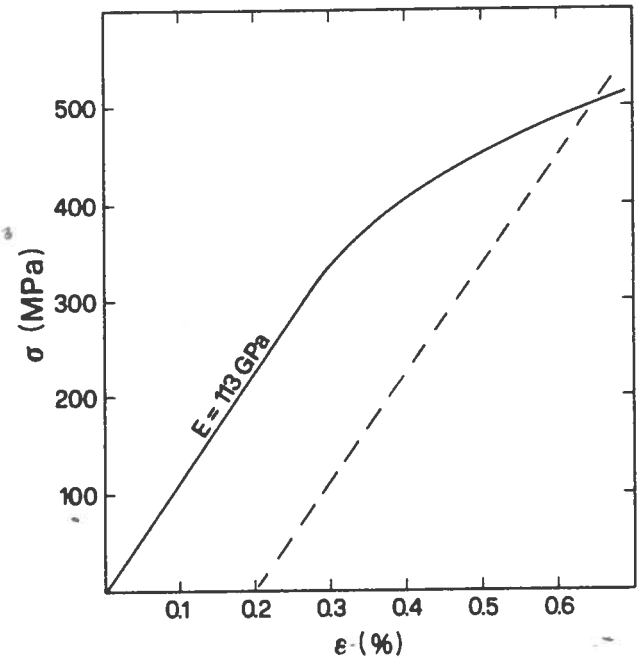

Fig.4 - Stress-strain diagram of superconducting insert as supplied by LMI. Insert is a monolithic flat cable ($1.8 \times 3.6 mm^2$) with Cu:NbTi=2:1. Measurements were performed at room temperature.

compressive stress on the cable and on G11 insulating strips of about 40 MPa.
The maximum hoop stress reached in the coils at full excitation is around 80 MPa, so at least 120 MPa of copper yield strength (2%) is required to be sure that cable works in elastic regime, whereas the RRR (residual resistivity ratio between 273 K and 4 K) needed for cryostability is around 160. As it will be shown in section II.1, this requirements are almost satisfied by choosing ETP copper with 2% of cold work.
When the β sections are negative supplied, the Lorentz radial force is inward and each turn have to be self-supporting. To give more radial compactness the interlayer insulator, 1x22 mm^2 G11 strips, are tensioned at about 600 N.
Because of the large axial prestress, the coils can go in "stick and slip" regime, see [5], and heat can be release between coils and cryostat midplane. To avoid this possible source of quench, friction tests between different materials were carried out and a 0.2 mm thick teflon sheet was inserted between G11 spacer insulators and cryostat plate (see section IV.4)

II - MEASUREMENTS ON THE SUPERCONDUCTING CABLE

II.1 Mechanical tests

In fig.3 and fig. 4 the stress-strain diagrams for matrix and superconducting insert are reported. The residual strain given by the axial compression of the coils was evaluated by measuring the sample shown in fig. 5. The results are reported in table III. The histogram of the unit length weight as measured on a 54 superconducting filaments sample is shown in fig.6. See figure captions for details.

TABLE III - Results of the axial stress tests

sample # → / axial stress ↓	1	2	3
60 MPa	6.5 μm	3 μm	5 μm
100 MPa	10 μm	7 μm	7 μm

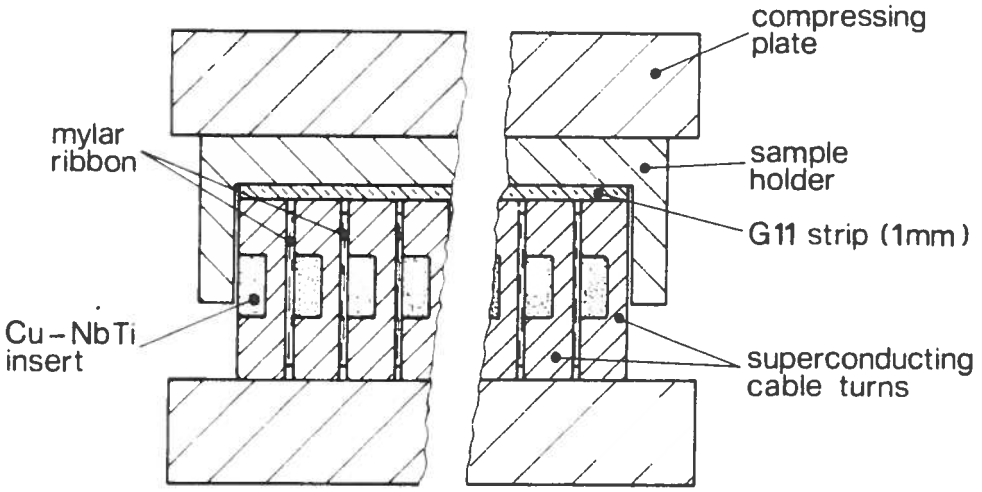

Fig.5 - Samples for the axial residual strain tests. The length of the cable pieces was 50 mm. After the pressure was applied and released, the height of the sample was measured. The sensitivity of the dial gauge were 1 μm, accuracy were about 3 μm. The best evaluation of residual strain at pressure we expect to have in the coil, nearly 41 MPa, is 3.3 μm (note that this value is very near to the accuracy of the measure, so probabily the true value is lower). Total residual shortening of the coils is 3.3 μm x 44 = 0.145 mm, corresponding to 0.024 % of residual strain.

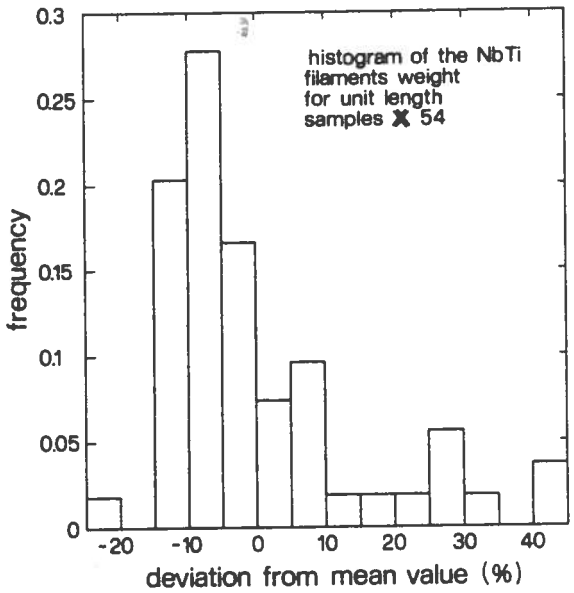

Fig.6 - In this figure is reported the histogram obtained by measuring the weight of 54 NbTi filaments. Weights were normalized to unit length; mean value was 28.1 mg/m and r.m.s. deviation from mean value was 4.1 mg/m. The total uncertainty of a single measure was $\pm$ 0.8 mg/m (3 % of mean value). By assuming a density for NbTi of 5.5, the calculated filaments mean diameter is about 80 μm. However more than half filaments (35) have a diameter around -10% of the mean value, so the great part of the filaments have a diameter of ~ 70 μm (= nominal value, see table II)

II.2 - Electrical tests

Electric resistance mesaurements were carried out on prototype samples of the cable.

The first sample, to which the results shown in fig.7 refer , was a 635 m long prototype that was cutted in three parts. The unit length resistance at room temperature of the first part was measured for the whole length; for the other two part only the unit resistance at the beginning and at the end was measured. This sample will be indicated in the following as sample # 1.

In fig.8 the residual resistivity ratio (which is an index of the copper impurity content) of the cable samples are plotted versus the cold work percentage.

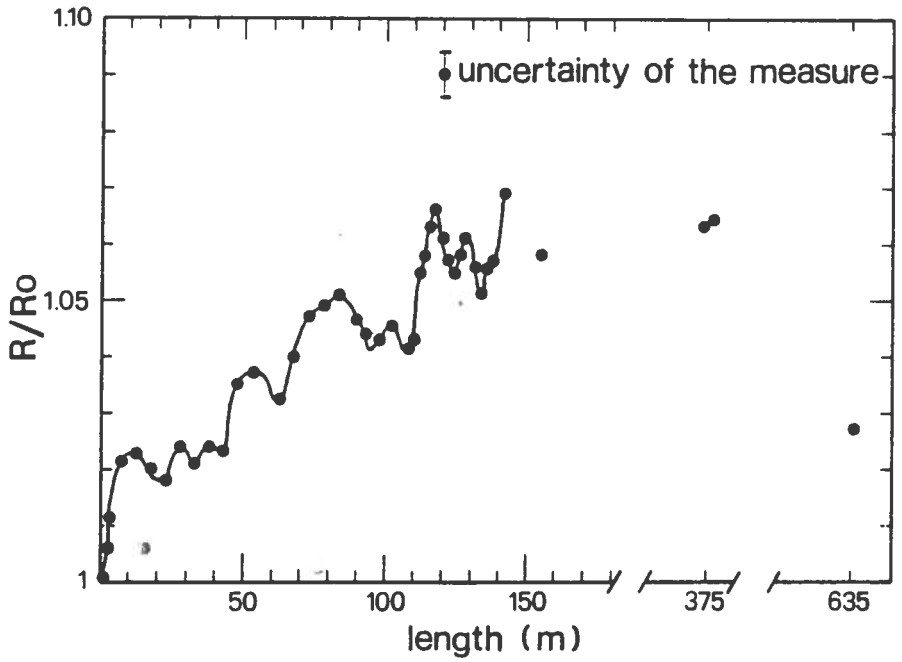

Fig.7 - In this figure the unit length resistance,at room temperature, of the first long protytpe of the superconducting insert is continuously plotted for the initial 150 m length; other point values are reported. The aim of the measure was to detect any relative variation of cross section of the superconductor, so the value are normalized to the initial resistance of the insert. The total accuracy of the measure was about ±4% mainly due to the temperature variation and power supply drift. The results seems to detect a decreasing of the cable cross section in the central part of the length respect to the beginning and the end. This effect was confirmed by the critical current measurements performed on this prototype (see fig.9 and the next para)

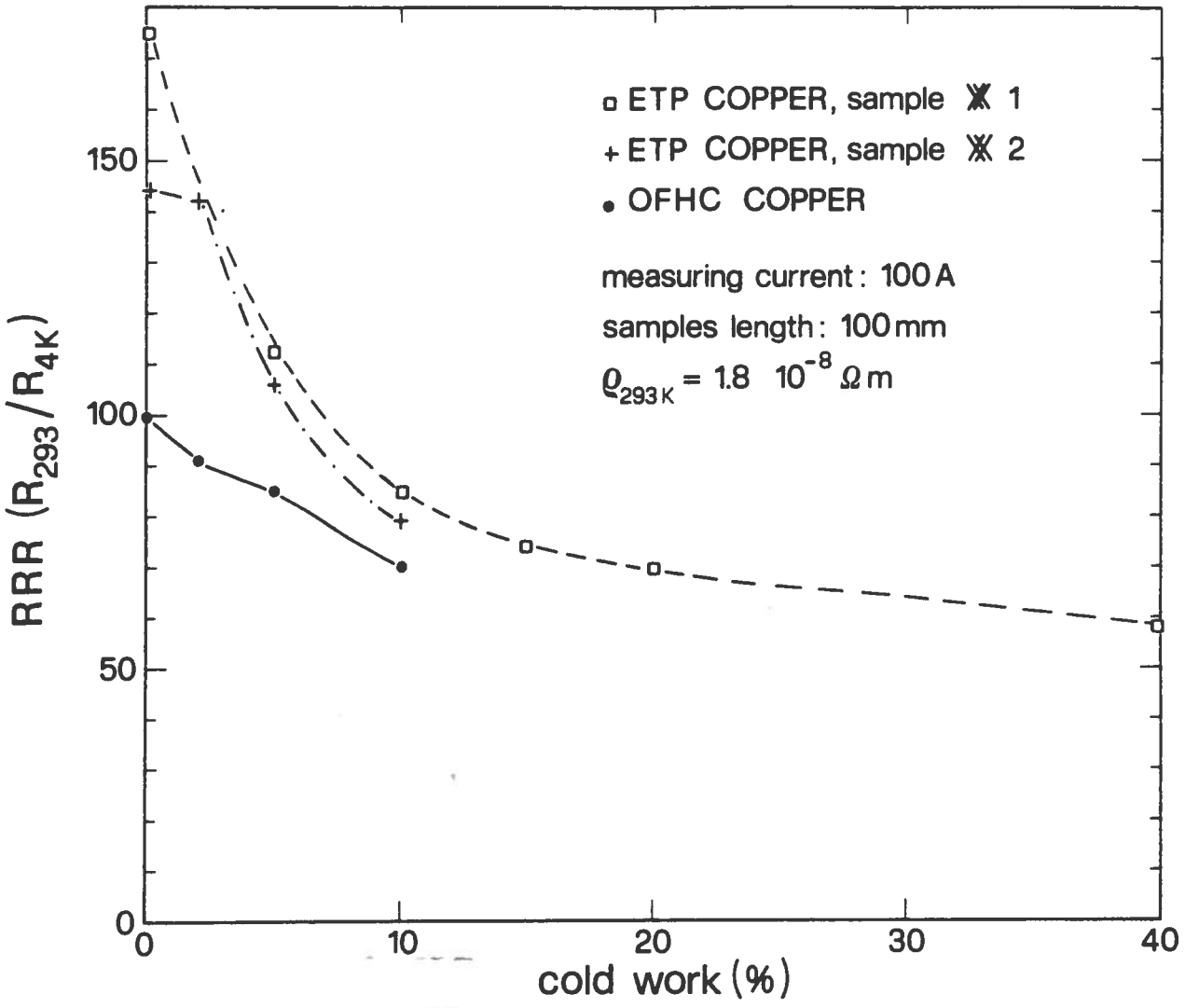

Fig.8 - Residual Resistivity Ratio (RRR) of different copper samples as given by LMI (supplier of the cable) [6]. Note that in this graph the RRR is ratio between resistivity at room temperature and LHe temperature; this value is 10% higher that the more usual ratio between resistivity at ice melting point and LHe. The final choice was for ETP copper with 2% of cold work grade. Complete chemical analysis of ETP copper by LMI is:

Ni ≤ 8 ppm
Sn = 9.2 ppm
Pb = 4 ppm
Fe = 1.5 ppm
Zn = 3.8 ppm
250 ppm ≤ O_2 ≤ 330 ppm

II.3 Critical current measurements

The critical current of different prototypes was measured [6] versus the field before starting cable production. The cable is required to carry 2700 A at 4.2 K with an external magnetic field of 5 T when this field is parallel to the largest size of the cable (see fig.9); moreover a Cu/NbTi ≈ 20 was chosen for stability, so the total cross section of superconductor is around 2.2 mm^2, that means more than 1200 A/mm^2 of superconductor critical current density at 4.2 K and 5 T.

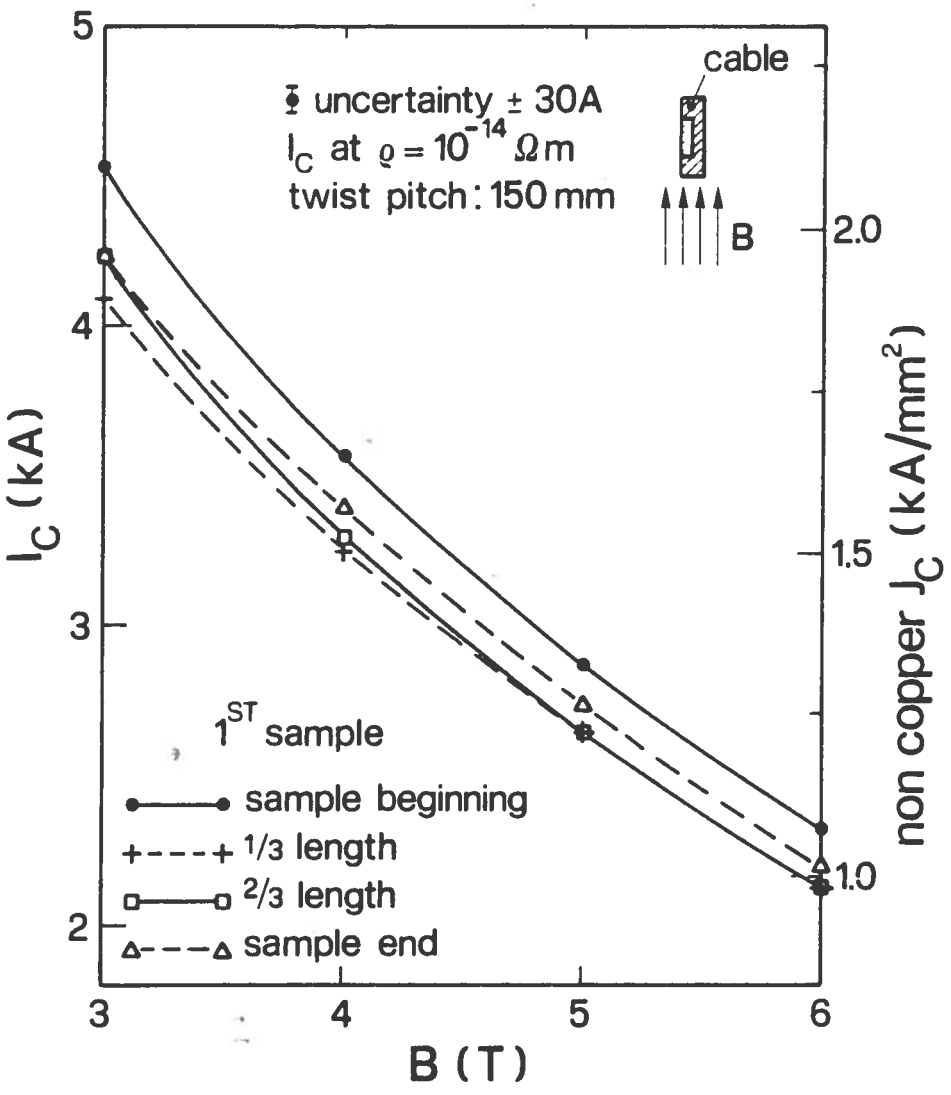

Fig.9 - Critical current versus the magnetic field for the first long sample of superconducting insert. The field direction is parallel to the largest size of cable, as it happens in the high field region of the coils.
Different curves refers at different position in prototype piece (total lenth is ≈ 630 m, see fig.7).

The results plotted from fig.9 to fig.12 refer to two different samples; the former, see fig.9 and fig.10, was a long length (≈530 m) prototype of the superconducting insert and it was mainly used to test the critical current curve versus the length of the cable. As shown in fig.9, variation in the critical current is within 10% at all field level.

The latter sample, much shorter than the previous one, has an higher critical current, as it's shown in fig.11.

Both these samples have shown an anisotropy of the pinning center; indeed when the field is parallel to the smallest cable face, the critical current shifts down 15%, as it is well shown in fig.12.

It is worthwhile to discuss the threshold for the critical current. In

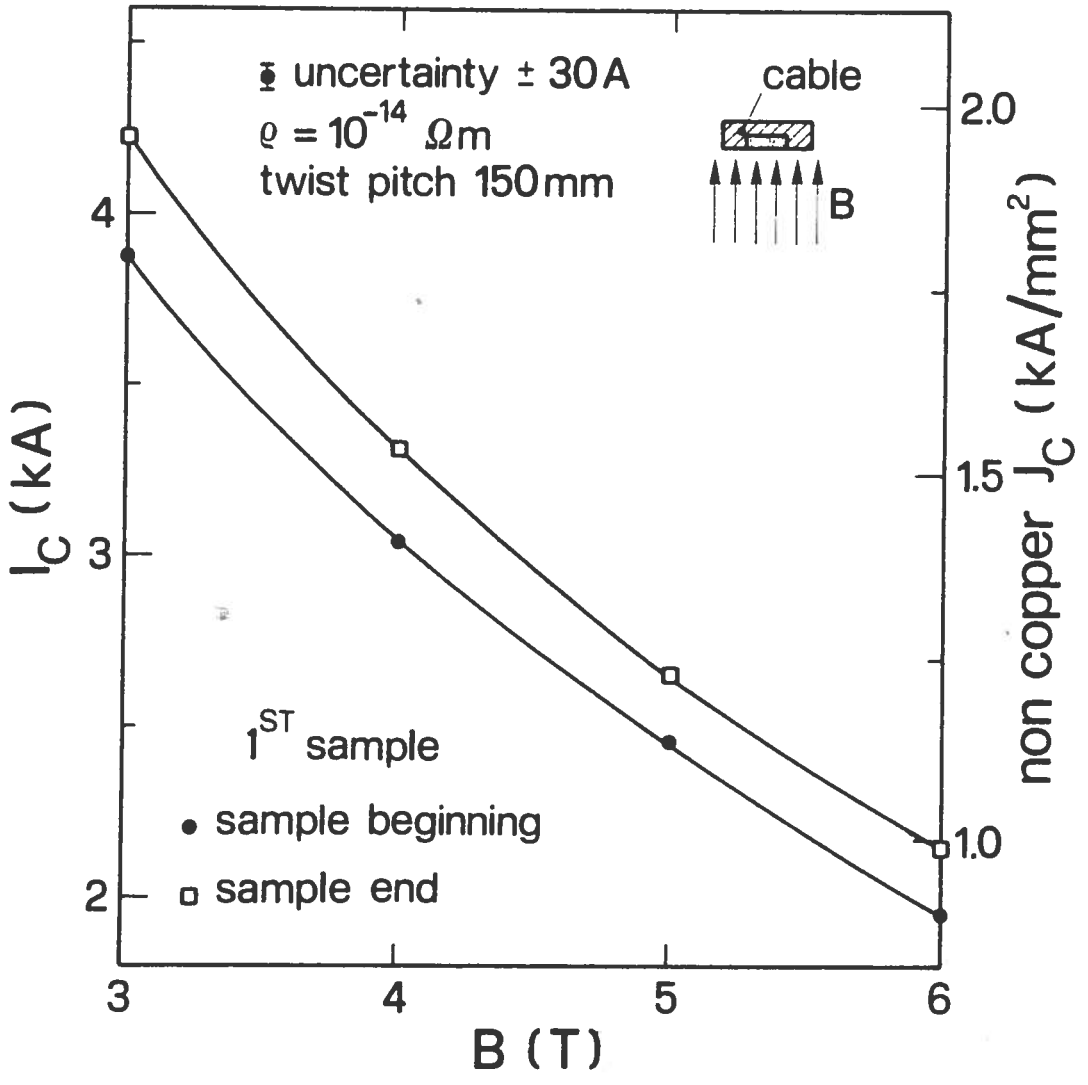

Fig.10- The same as in fig.9 but with field parallel to the smallest size of cable.

the measurements on prototype, the superconductor apparent resistivity criterion was adopted with $\rho_c = 10^{-14}$ Ωm; taking in account that at 5 Tesla J_c(non copper) is about 1.5 kA/mm^2, see fig.11, the corresponding electric field is $E_c = J\ \rho_c = 0.1\ \mu V/cm$, well under the usual 1 μV/cm threshold. So the critical current was measured for the second sample with the $\rho_c = 10^{-13}$ Ωm criterion and it was found to be about 4 ÷ 5 % higher than with the 10^{-14} Ωm threshold. In the following measures the 10^{-14} Ωm threshold was restored.
In the fig.13 the results of the critical current measurements carried out on two short samples (beginning and end) for every piece length

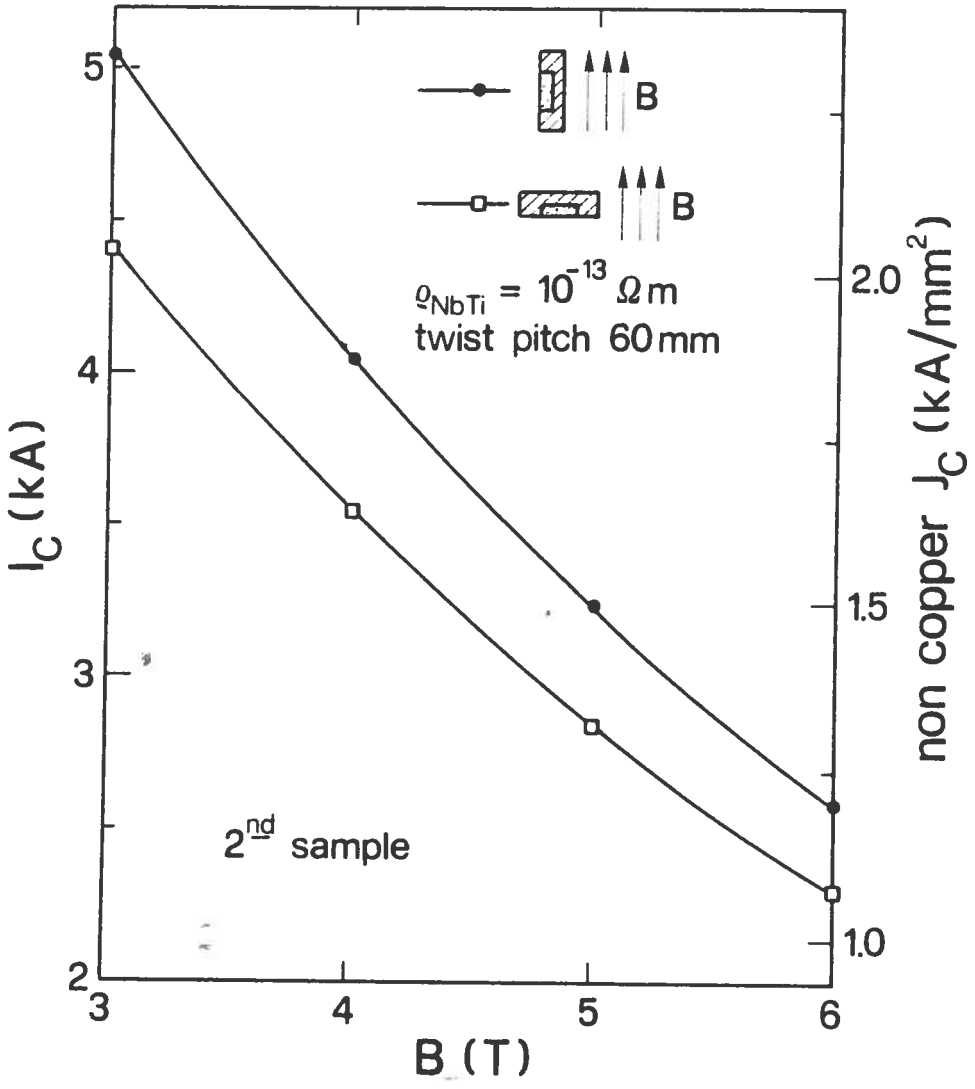

Fig.11-Critical current versus B of the second sample (short sample).

used for the coils winding are shown [6]. The shaded area gives an idea of the large spread of the values. Pointing out the fact that every piece has reached the required performance (2700 A at 5 T), we attempt some explanation for such a large spread. The lines a and b are typical performance of short sample of the first set delivered by LMI; it was followed by a set of short samples showing lower characteristics, within b and c lines. Perhaps, due to very comfortable results on the first set, care in production was lessened and/or a small reduction in NbTi cross section was taken. Whatever the cause of this remarkable degradation, the third (and last) set of short samples delivered by LMI showed better performaces than the second set, without reaching the initial value; typical value for this short sample set were near the b line.

However we have to take in account of some troubles in the measuring apparatus (6). Spurious signals rised because of the large electromagnetic forces exerted on the sample holder (six samples were measured together every time). These troubles were more effective at higher current, so for some samples the results were not the critical current but the maximum attained current.

Critical current measurements were done by the STIPE-CEN CEA of Saclay, France, in the frame of an official agreement between the Cyclotron Laboratory and STIPE Laboratory. The measures performed by STIPE laboratory are listed in the conclusions.

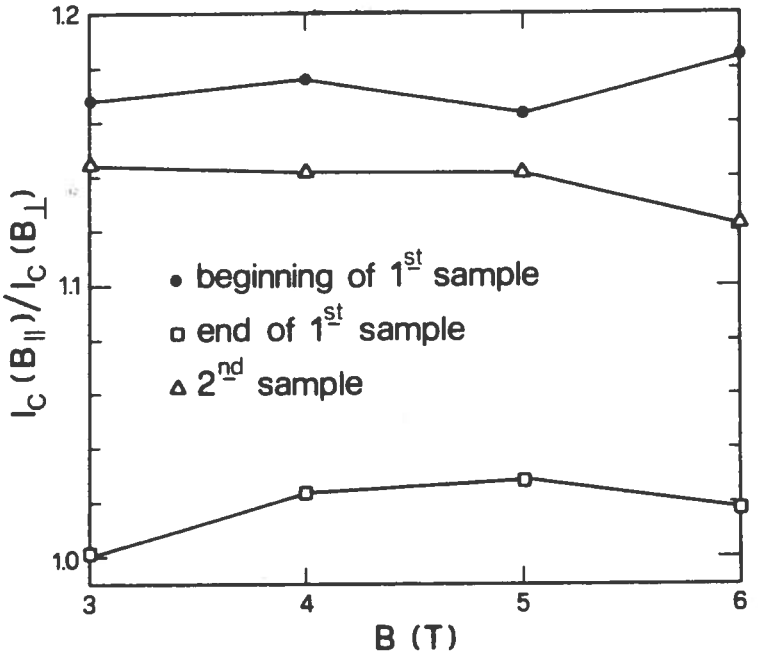

Fig.12- Ratio of the critical currents with different field directions. See figs.9,10,11 and text for details.

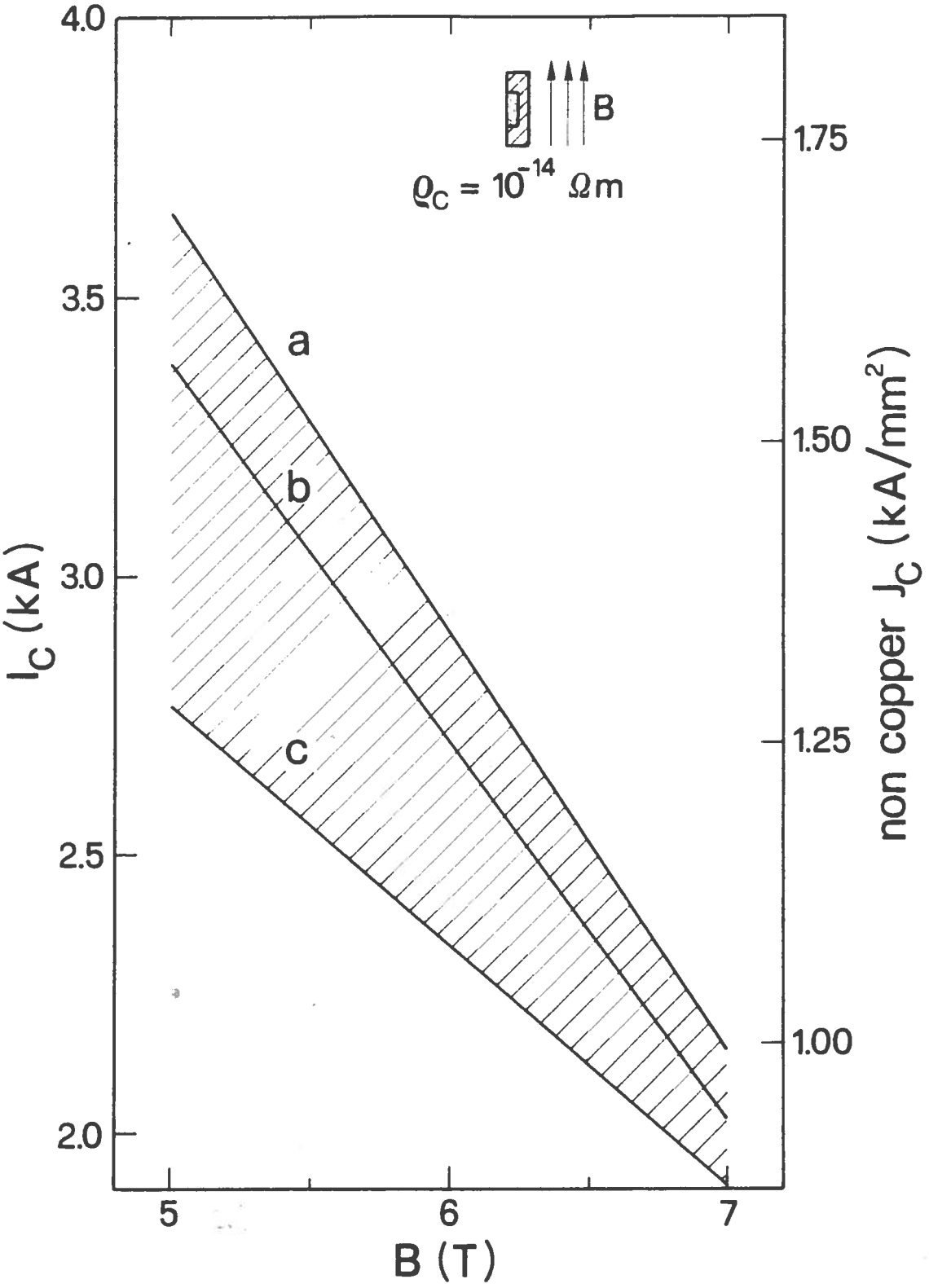

Fig.13- Critical current versus B for the short samples (1 m) of superconducting insert used for the coils. Two short samples were cutted (beginning and end) from each double pancake piece. Samples number is 96. Shaded area indicates the spreads of results, see text for details.

III - MEASUREMENTS ON STRUCTURAL MATERIALS

III.1 - Mechanical tests on Beryllium Copper (2%)

This material was employed for the rods that prestress the coils, see fig.2 and cap.I. Beryllium copper was chosen because of it excellent mechanical properties (also at low temperature) and, above all, because its thermal contraction is very near to the coils one,so avoiding an excessive release of the prestressing rods after the coils cool-down.

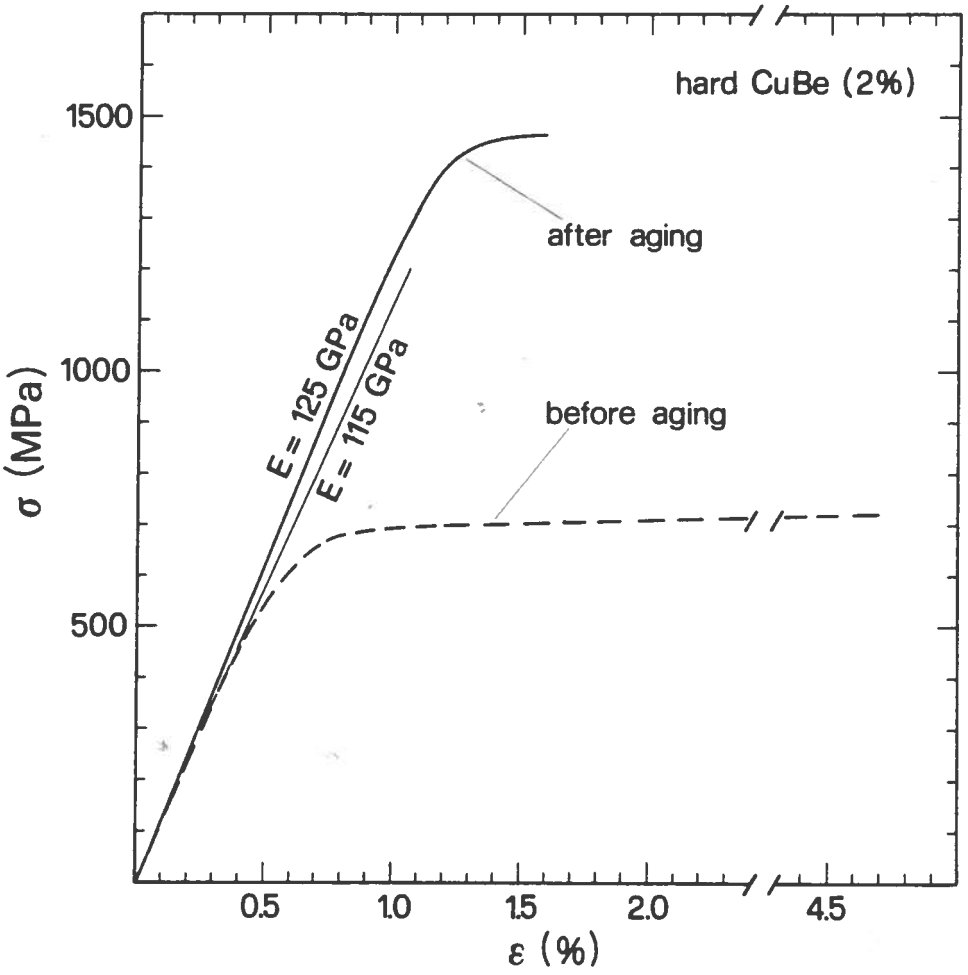

Fig.14- Stress-strain diagram (at room temperature) of a prototype CuBe bar. Material was supplied by Vacuum Schmeltze (Hanau-D) in the non aged form. Aging was performed in the lab, 325 C for 1 h. Note that yield strength is very near to the tensile strength. The diagram refer to the best sample, and it must be pointed that the rupture el ɔngation is a bit more than the reported value; in fact before rupture the strain gage became unreliable. The worst samples of this first set of bars gave the following results: yield strength = 1181 MPa, tensile strength : 1275 MPa, elongation : 3.9 %

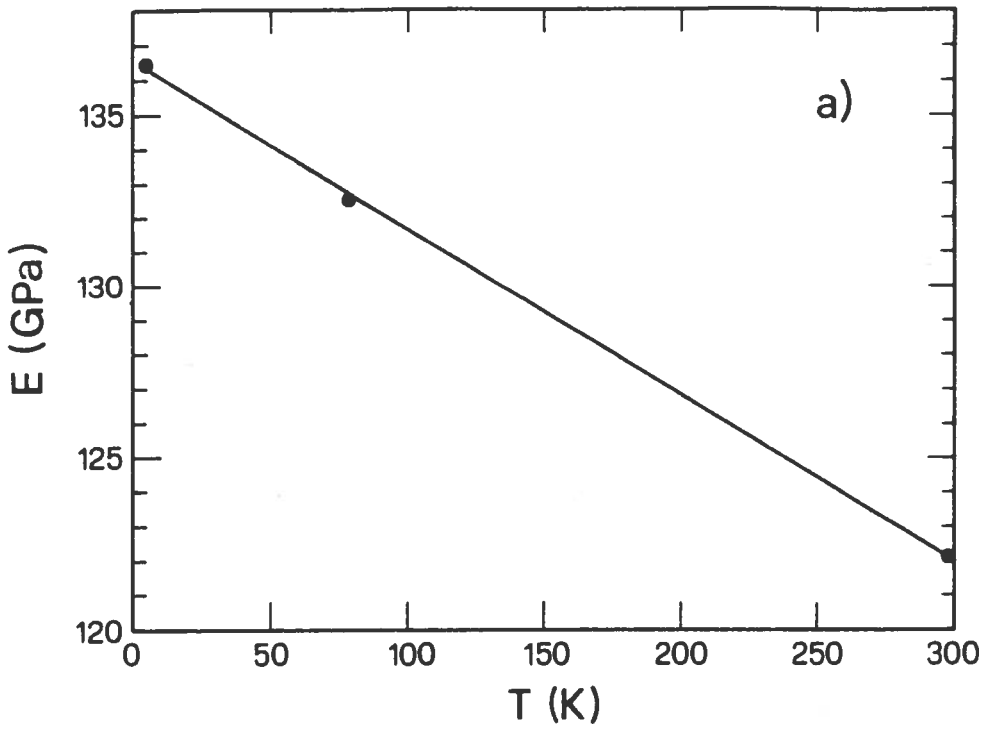

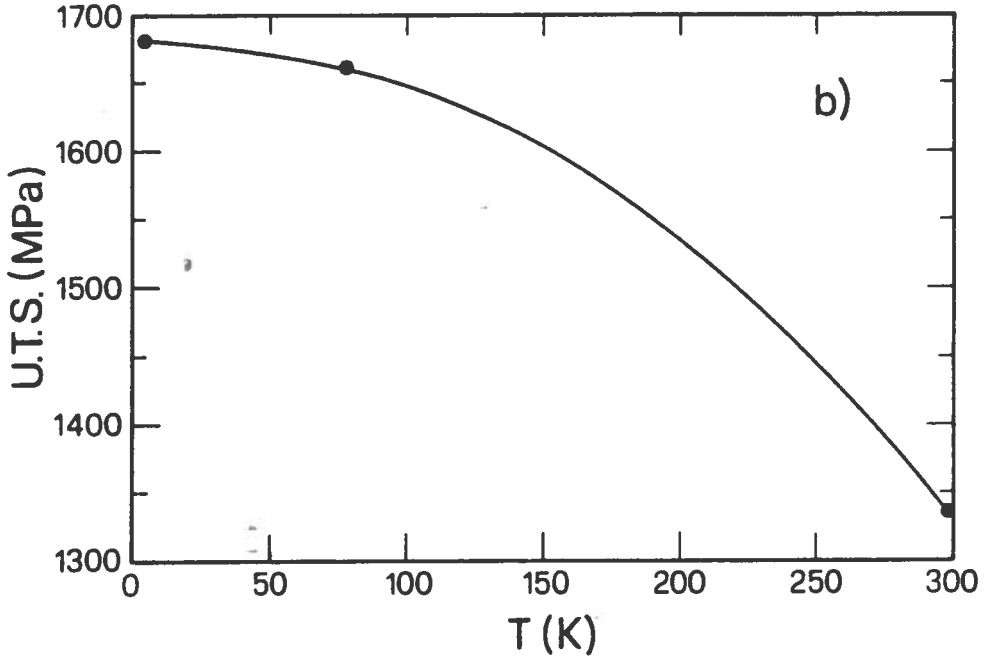

Fig.15- Elastic modulus (a) and ultimate tensile strength (b) versus temperature for the CuBe (7). This samples were supplied by Vacuum Schmeltze in the aged form; the characteristics are a bit lower than one reported in the previous figure.

III.2 - Mechanical tests on AISI 316 L

This material is used for the midplane plate that supports and splits the coils, see fig.2; to allow beam injection and extraction, a lot of radial channels are drilled in this plate; calculations foresee a maximum working point a bit more than 100 MPa. Results of room temperature mechanical tests are given in the following table IV.

TABLE IV - mechanical properties of AISI 316 L

stress direction ↓	0.2% yield strength (MPa)	tensile strength (MPa)	elongation (%)	impact test KCU (J/m^2)
longitudinal	232	545	57	$2.16\ 10^6$
trasversal	229	548	60	$1.76\ 10^6$

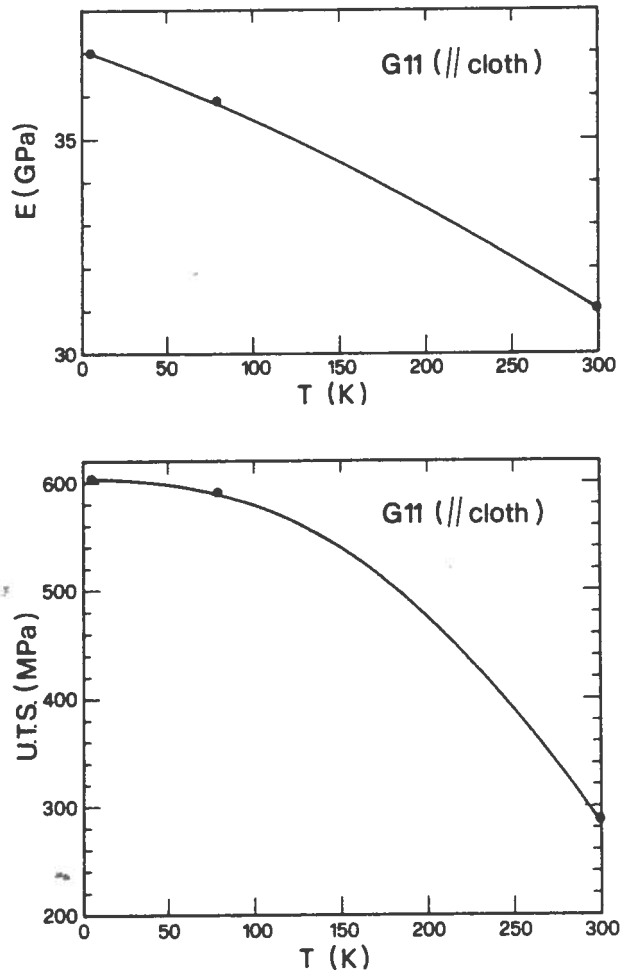

Fig.16- Elastic modulus and tensile strength versus temperature for G11 [7]. Specimens were supplied by Simpres, Lissone (Mi) - I; G11 was used for layer to layer insulators; tension was applied in the warp direction.

III.3 - Mechanical tests on G11 and mylar ribbon.

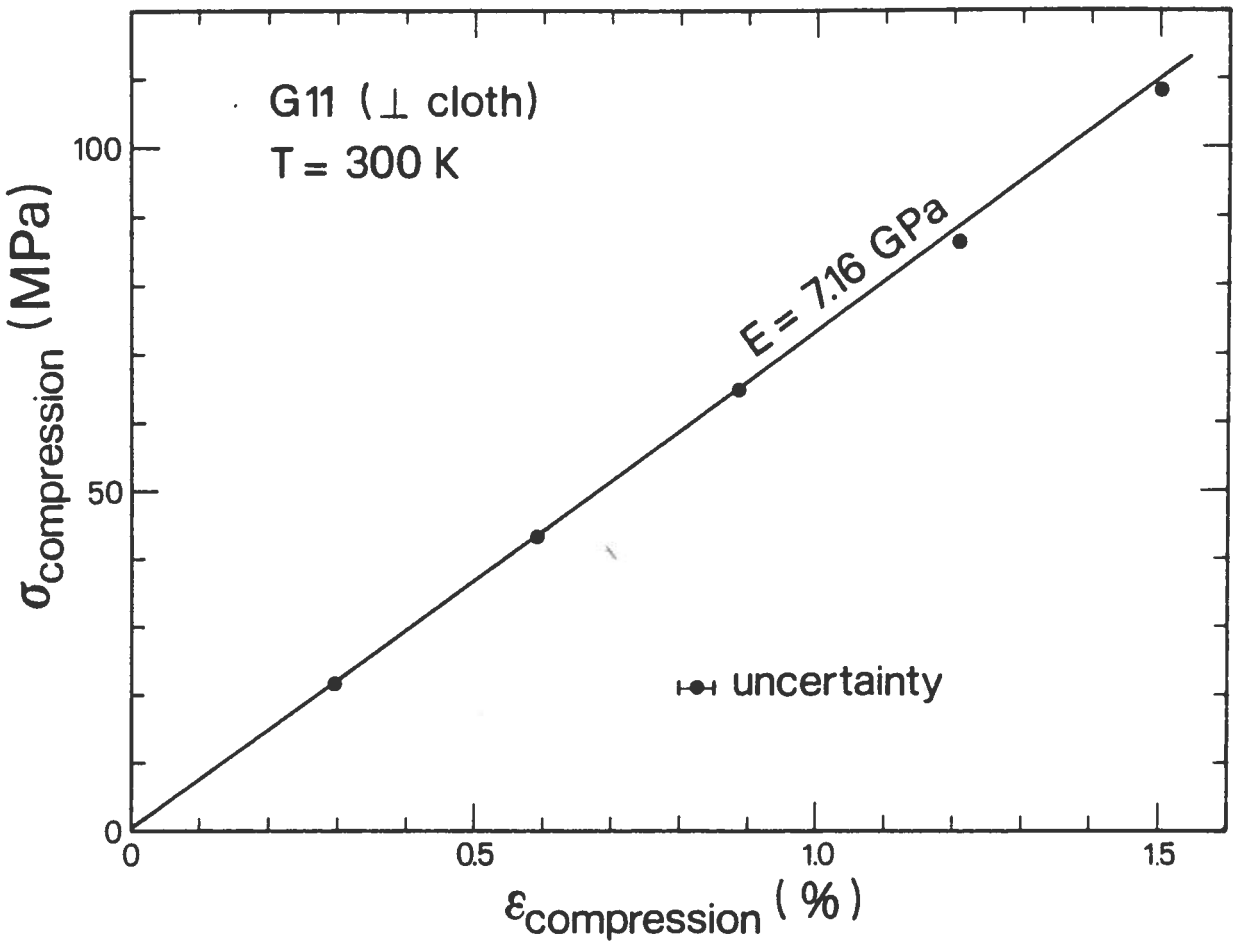

Fig.17- Stress-strain diagram for G11 at room temperature; force was compressive and perpendicular to the glass cloth. The results indicate that untill this stress level the material is nearly elastic (during operation calculated maximum stress is 55 MPa); after compression releasing no permanent deformatio ns was detected. Uncertainty was ± 0.6 MPa for stress and ± 0.02 % for strain.

We have carried out one mechanical test, at room temperature, on mylar ribbon used for turn to turn insulation. We applied 157 N to the backing strip, 11 mm wide and 0.125 mm thick, for a long time; strain was 8.7 % and permanent deformation was 4.3 %.

III.4 - Thermal expansion measurements on CuBe, G11, TiAl6V4, Mylar, Teflon, Cu, carbon fiber, Al.

Thermal expansion of some material versus temperature was measured [7] and results are shown in fig.18.
Experimental values were fitted by means of 4th order polynome

$$\Delta L/L_0 = A_0+A_1 t+A_2 t^2+A_3 t^3+A_4 t^4$$

where the reference length L_0 is given at 293.15 K and t=T(K)-293.15.

	CuBe	TiAl6V4	G11(warp)	G11(fill)
A_0	-9.42911E-7	3.3413 E-6	-1.17199E-6	-6.60604E-7
A_1	1.57139E-5	7.81649E-6	1.23142E-5	1.39366E-5
A_2	9.1146 E-9	-1.02683E-8	1.30287E-9	1.9527 E-8
A_3	3.74417E-13	-8.09789E-11	4.95619E-11	1.08056E-10
A_4	2.36873E-13	-8.09789E-14	1.51794E-13	3.43574E-13
max error	1.12E-6	1.48E-6	8.76E-6	9.76E-6

These values may be compared with the results of the total expansion between room temperature and LN temperature as measured in our lab. Our measurements are reported in the following table V.

TABLE V - RT+LNT thermal expansion

material	# of measurements	-ΔL/L (ppm)	uncertainty (ppm)
ETP copper (sc cable)	2	3000	100
CuBe (2%)	5	2900	50
G11 warp (*)	11	2120	50
G11 warp (**)	3	2170	80
G11 fill (*)	7	2450	50
G11 ⊥ to glass cloth (*)	5	4280	50
G11 ∥ to glass cloth (**)	3	5150	50
Anticorodal	2	4050	5
Mylar (thickness)	7	19000	500
carbon fiber cloth	8	230	90
Polyester with glass	3	4200	100

(*) this material was 1 mm thick strip (for interlayer insulation)
(**) this material was 10 mm thick, used to lock sc cable ends

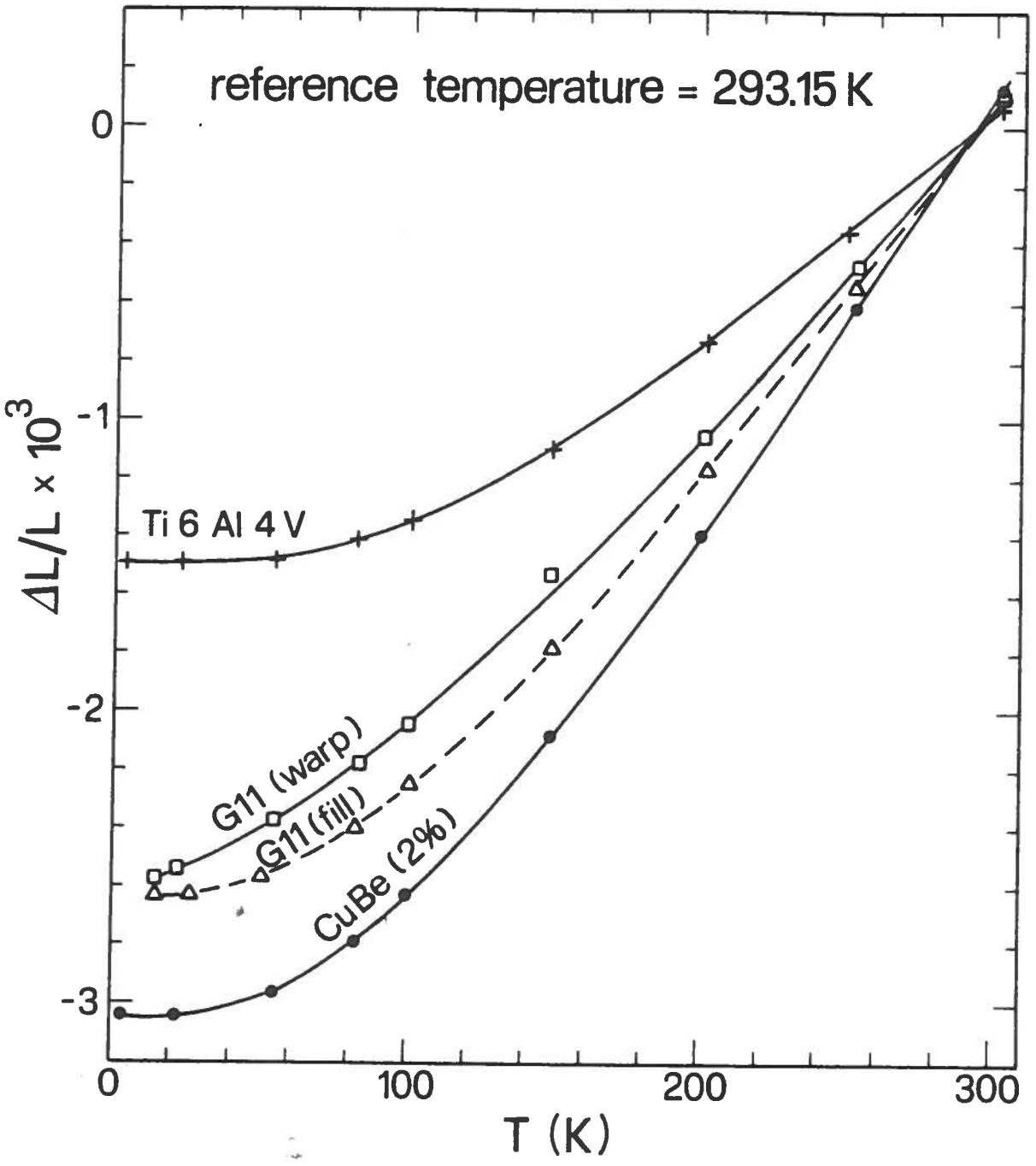

Fig.18- In this graph the thermal expansion versus the temperature is plotted for some materials used in the coils assembly. The accuracy of the measurements was evaluated to be ± 1 % [7].

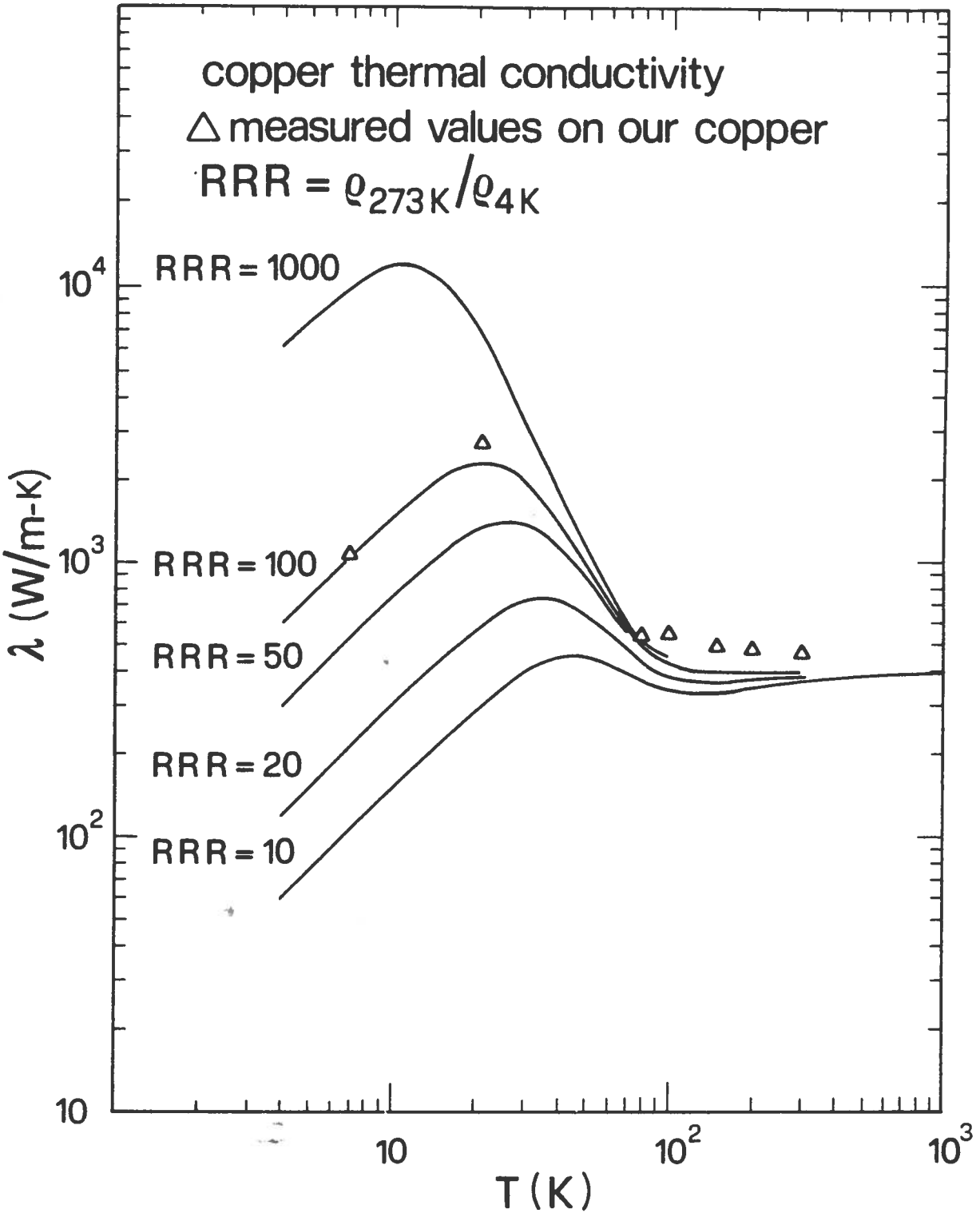

Fig.19- Triangles indicate thermal conductivity measures for the ETP copper used for the current leads of the superconducting coils (7). The residual resistivity ratio (here defined as $\rho_{273}/\rho_{4.2}$) for the copper was RRR = 120 (≃ RRR = 100 at B = 1 T). Solid lines are reported from literature (8).

IV - TESTS ON SYSTEMS

IV.1 - Tests on electrical junctions

A sketch of the electrical junctions between double pancakes is shown in fig.20, where the measurements of their resistance versus magnetic field is reported, too. The curves from A to D refer to following junction arrangements:

curve A:the cables are only mechanically pressed by means of six stainless steel screws (about 10 kN each screw); junction length is 70 mm;

curve B:the cables are pressed with a 0.6 mm thick InAg(2%) foil between the cables;

curve C:the InAg foil is melted, so the cables are soldered and after they are pressed by the screws;

curve D:almost the same of curve C; difference are a bit increase of the Silver content in the soldering, InAg(4%), and increasing of soldering lenth to 80 mm.

InAg alloy was used instead of the more usual SnPb because of its low melting temperature (140 C against 220 C of SnPb); it is worthwhile to recall that superconducting insert is soft soldered into the grooved copper matrix by means of SnPb, so we were forced to not exceed 200 C during the junction soldering.
In fig.21 the voltage - current characteristics at zero Tesla for the extreme arrangements (A and D) are shown. The non linearity of the curve is well marked for the case with no soldering and it can be detected also for the low current part of the curve D. This deviation from linear behaviour disappears when a small magnetic field is superimposed.

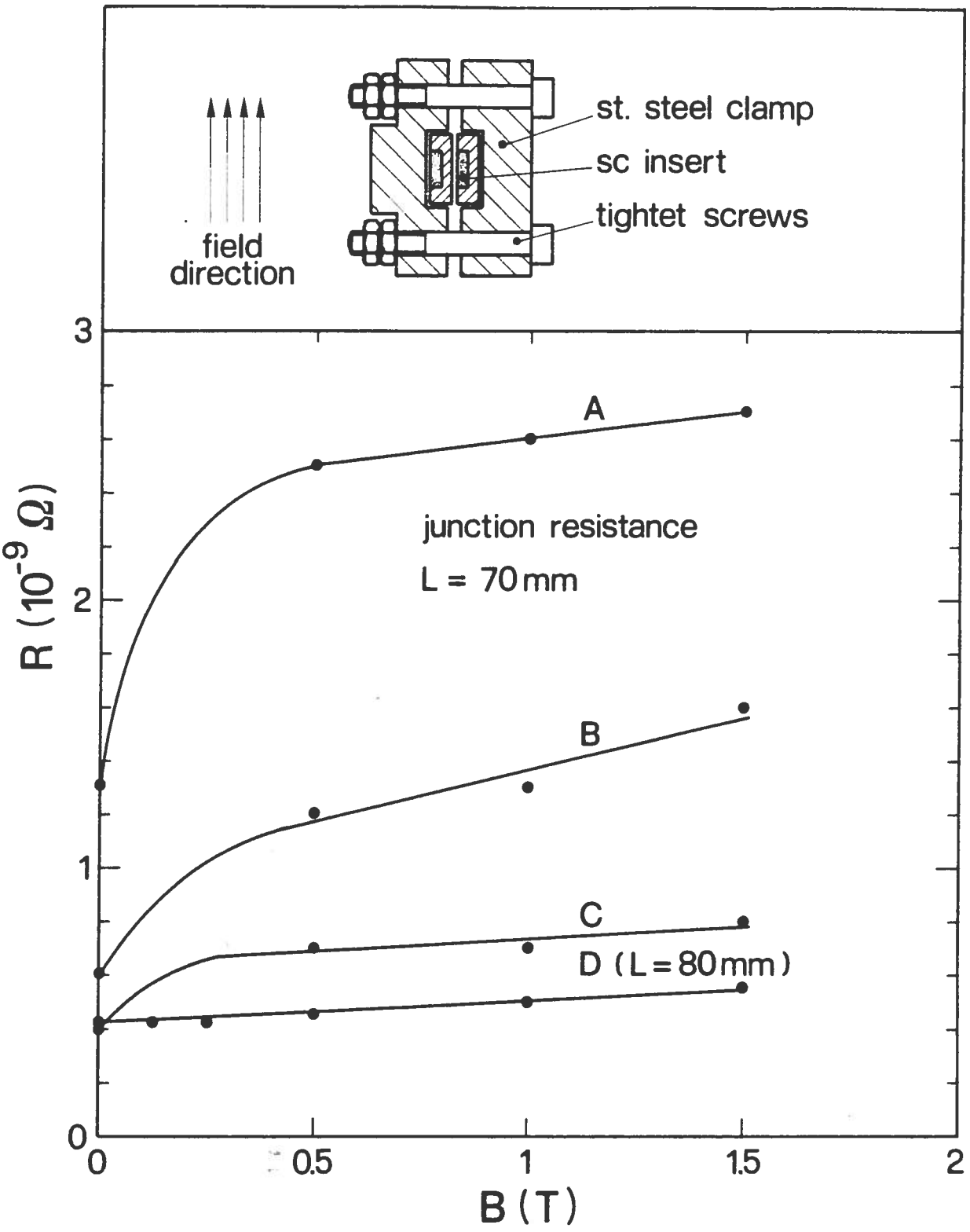

Fig.20- Sketch of the electric junction between the double pancakes and electric resistance versus magnetic field. Different curves refer to different arrangement of the stainless steel vice, see text for details.

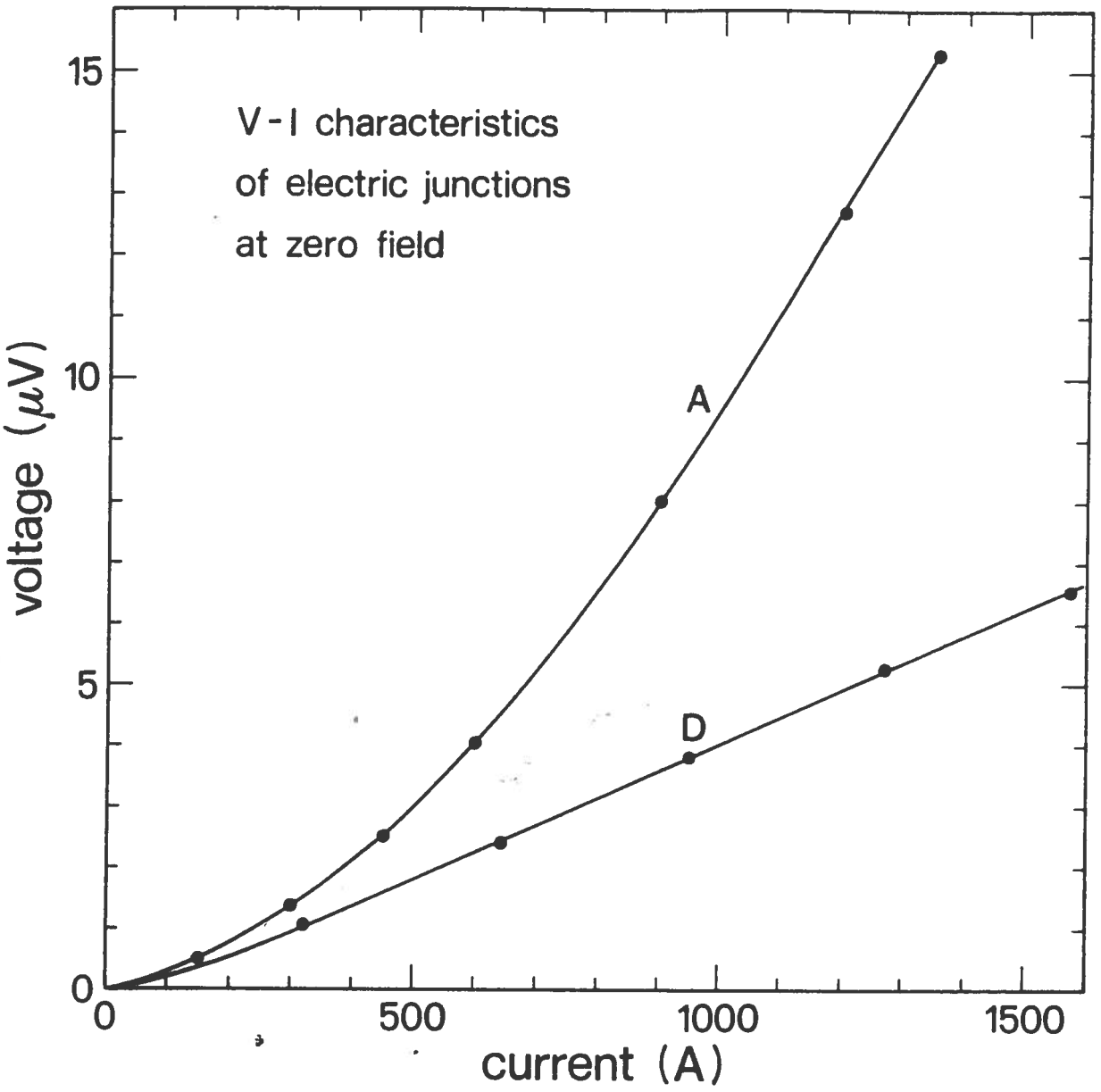

Fig.21- Voltage-current plot at B = 0 T for two junction arrangements: with mechanical pressure only (A) and with soft soldering followed by pressing (D).

IV.2 Tests on the bonding strength on G11 insulators.

The G11 strips used for interlayer insulation are tensioned to about 600 N, to contribute to the radial stiffness of the coils, by means of bonded G11 clamps, see fig.1. During the winding of two double pancakes prototypes, in which the clamps were bonded without pegs,

this bonding reported several damages, emphasized also by the LN cool-down test.

Following this a lot of tests on bonding shear strength between strips and clamps were carried out with different aging cure (typical: five days at room temperature or 1 h at 80 C) and under different test condition (pure tension or tension + torque).

Tests emphasized that bonding was not very reliable: some samples shown high strength but other samples were weaker and some other shown very poor bonding strength.

This spread in the results was probably caused by operator inaccuracy and by use of expired bond (bond was Hysol AE 934). So we decided to insert a fiberglass peg, see fig.1, and this raised the shear strength to quite comfortable values.

In the following table the results are reported (the bonding surface was about 220 mm^2).

TABLE VI - shear strength of G11-G11 bonding

#	rupture strength (kN)	test condition(*)	notes
1	1.4	T	
2	2.1	T	after 5 LN shocks
3	2.1	T	idem
4	1.6	T	
5	0.6	M	
6	0.6	T	
7	1.3	M	
8	0.6	T	
9÷14	$\leq$0.5	T	these were aged only two days at room temperature; bond was used a bit after the expiration time
15	$\leq$0.5	M	1 day room temperature of aging
16	$\leq$0.5	M	
17	0.7	M	
18+19	$\geq$3.2	T	with peg (aged in oven)
20+21	$\geq$3.2	T	idem
22	0.5	T	without peg (aged in oven)
23	1.2	T	idem
24	0.8	T	idem
25	0.7	T	idem
26	$\geq$1.0(**)	M	with peg (aged in oven) and after 5 LN shocks
27	$\geq$1.0(**)	M	idem
28+29	$\geq$3.8	T	idem

(*) T = pure tension
M = tension + torque
(**) rupture was not determined by peg but by strip tear.

IV.3 - Mechanical tests on the last double pancake turn.

During the winding the superconducting cable was tensioned, at about 35 MPa (1.6 kN) and so it was the stainless steel tape inserted in last eight turns, at about 150 MPa (2.9 kN), see cap.II and V. The stainless steel U-shaped clamps, shown in fig.1, were expected to lock the cable and to avoid unwanted sliding between the last turns with consequent tension loss.

Following severe tests carried out on the two prototype pancakes, the last turn was found to have slided of about 1.5 mm inside the U clampss.

Some adhesives were investigate to attempt a bonding between the end of the last st. steel turn, welded to the U clamps, and the last superconductor turn; we recall the strict condition for this bonding: no possibility to have any cure, resistance to several LHe thermal shock, reliability for an industrial grade accuracy.

The maximum strength was reached by using STYCAST, as supplied by ANSALDO COMPONENTI (Genoa - I) and was near 2 kN at room temperature, but fell abrubtly to 0.5 kN after five LN thermal shocks.

Because of the previous results, we decided to have a mechanical lock. This was carried out by means of a G11 square, fixed to the cable by four st. steel ϕ2 screws; when the cable is released this square pushes against the U clamps avoiding the sliding as it may be seen in fig.22.

Tests shown that strength of this system is over 5 kN in any condition, so this arragenments was adopted.

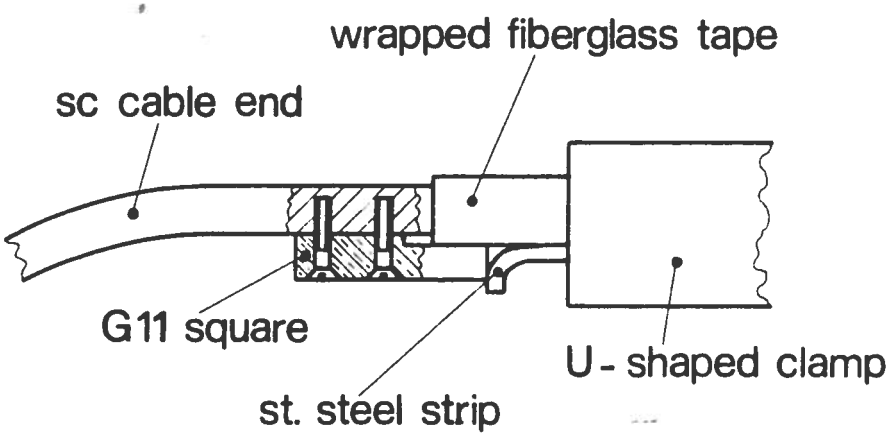

Fig.22- Top view of the pancake end with the locking square (see fig.1 for a vertical section without square).

IV.4 Friction test.

The superconducting coils are splitted in the median plane by an AISI 316 L plate, see fig.2; to avoid heat release in the cable, see cap.II and ref.[5], we carried out some tests with different insulators between the coils and the plate.
The experimental apparatus is sketched in fig.23, where is reported the first arrangement with just only G11 insulator. In this case we found that friction between G11 and coils is less than G11 and st.steel plate.
To avoid this we checked G11 sheet with one tefloned surface; another test was done by using G11 sheet with one surface covered by molybdenum bisulfide (MoS_2).
These tests were invariably negative: slips began between cable and G11 instead of beginning between st.steel plate and teflon or MoS_2 treated face of G11 sheet.
Good results were achieved by inserting a teflon sheet, about 0.2 mm thick, between the G11 insulator and the st.steel plate. In this case, whatever force we applied, the coils and G11 moved together and G11 slips on the plate. Moreover, in the first slipping teflon is extruded so covering in a very good way the the surfaces; indeed taking away the teflon sheet the stick and slip happened between insulator and the plate.
Following these tests we decided to insert a 0.2 mm teflon foil between G11 insulator and the AISI 316 L plate of the cryostat and between the separators of the α and β sections.

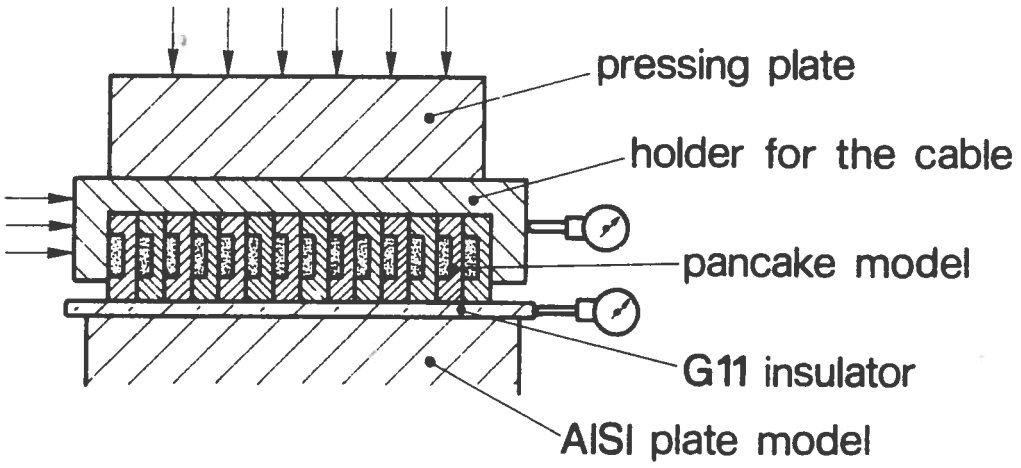

Fig.23- Draft of the assembly used for the slippage tests.

IV.5 - Test of the coils axial prestressing system.

A model of the axial prestressing system of the superconducting coils was built in the laboratory, to test procedure, feasibility, accuracy of the operations and to have some experimental check about dimension of the CuBe rods and of the st.steel plate.
The model is about 90 cm long and straightform with 11 inner CuBe rods (ϕ=10 mm) and 6 outer CuBe rods (ϕ=14 mm). The bottom AISI 316 L plate has the same profile as in the cryostat, see fig.2 and fig.24, and the top plate, AISI 316 L too, was 35 mm thick; the coils were simulated by two anticorodal parallelepipeds.
After first measurements we decided to reduce the top plate thickness to 25 mm; the results, shown in fig.24 together the experimental apparatus, indicate that plate bending gives a rise of -0.29-(-0.16) = -0.13 mm. This plate thickness was chosen for the coils prestressing plate.

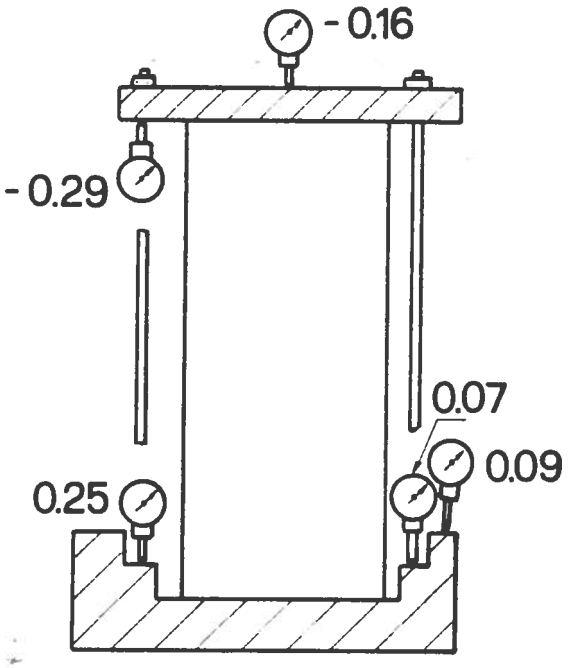

Fig.24- Top: picture of model of the axial prestressing system, with the dial gauges and the hydraulic jack to tension the CuBe tie-rods (to understand better see also fig.2).
Bottom: selfexplanatory view of the displacements (in mm) of the measured points at maximum load; negative valuee indicate downward displacements and viceversa.

V - MEASUREMENTS ON DOUBLE PANCAKES PROTOTYPES

V.1 - Strain measurements during the mandrel release.

The stress profile in the pancakes was deeply studied in every phase (winding, mandrel release, cool down, field on). Results are reported in ref [2]; we only recall the summarizing graph reported in fig.25. During the winding of the two prototypes we bonded eight strain gages on the 3.5 mm wide side of the cable and one strain gage on the last turn of the stainless steel banding tape. The main aim was to measure

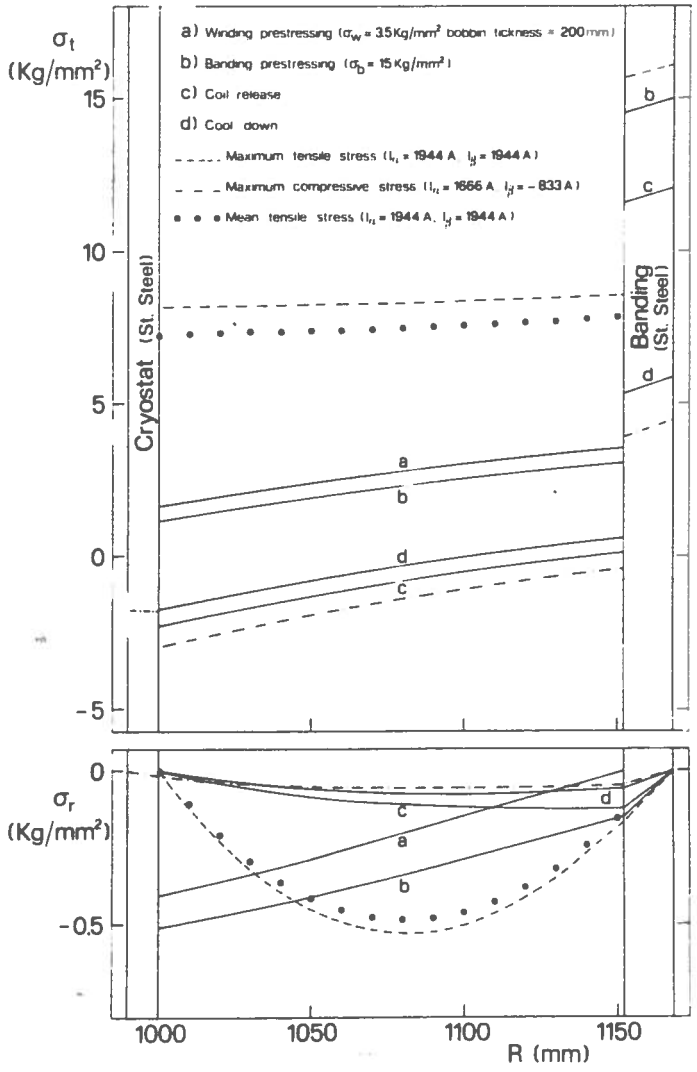

Fig.25- Calculated hoop (σ_t) and radial (σ_r) stresses in the coils versus the radius in every phase from winding untill field on.

the release in the pancakes to the mandrel taking off and to compare these measurements with the calculation shown in fig.25. To be precise we measured the difference between the curves b and c of the tangential stress reported in fig.25 in term of strain.
Theoretical calculations were carried out by assuming: a) the cable workes always in elastic regime; b) the banding is an external restraining cylinder.
Fig.26 shows the results for the former prototype and fig.27 for the latter one. Regardless the extreme positions, the behaviour is similar to the expected one but the values for the first prototype are about 40 % lower than the calculated ones.

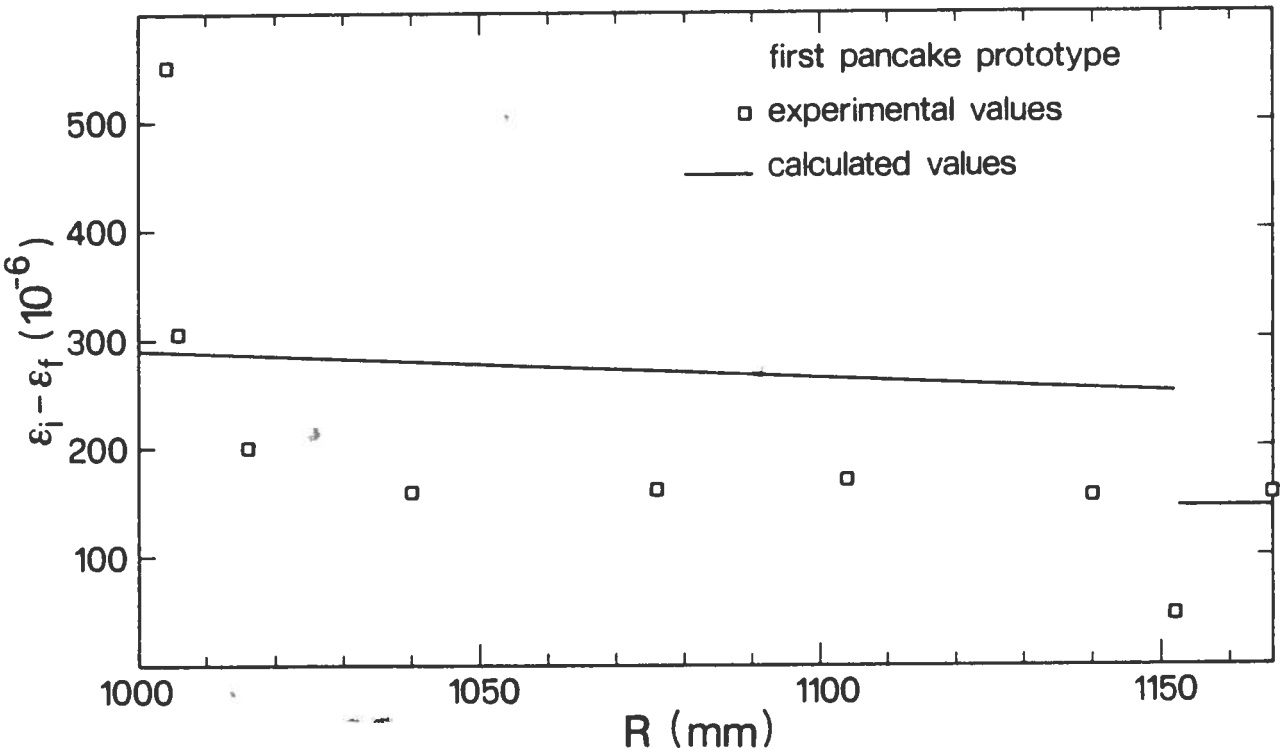

Fig.26- Difference between tangential strain before (ε_i) and after (ε_f) mandrel release of the first prototype. Strain is in ppm.

During the winding, tension releases were detected and above all the mandrel release was done in a too sharp way. More care was taken in the winding of the second pancake and a smother procedure for the mandrel release was adopted, giving the good results shown in fig.27. The residual differences between expected and measured are probably due to experimental uncertanty, to have attained initial plastic regime of the cable (full copper for the prototype) and to some difference between the behaviour of "continuos" pancake model used for calculations and the behaviour of "discrete turn" real pancake. Strong difference shown in fig.26 at the extremes is due to singularities as layer to layer jump and welded st. steel U clamps.

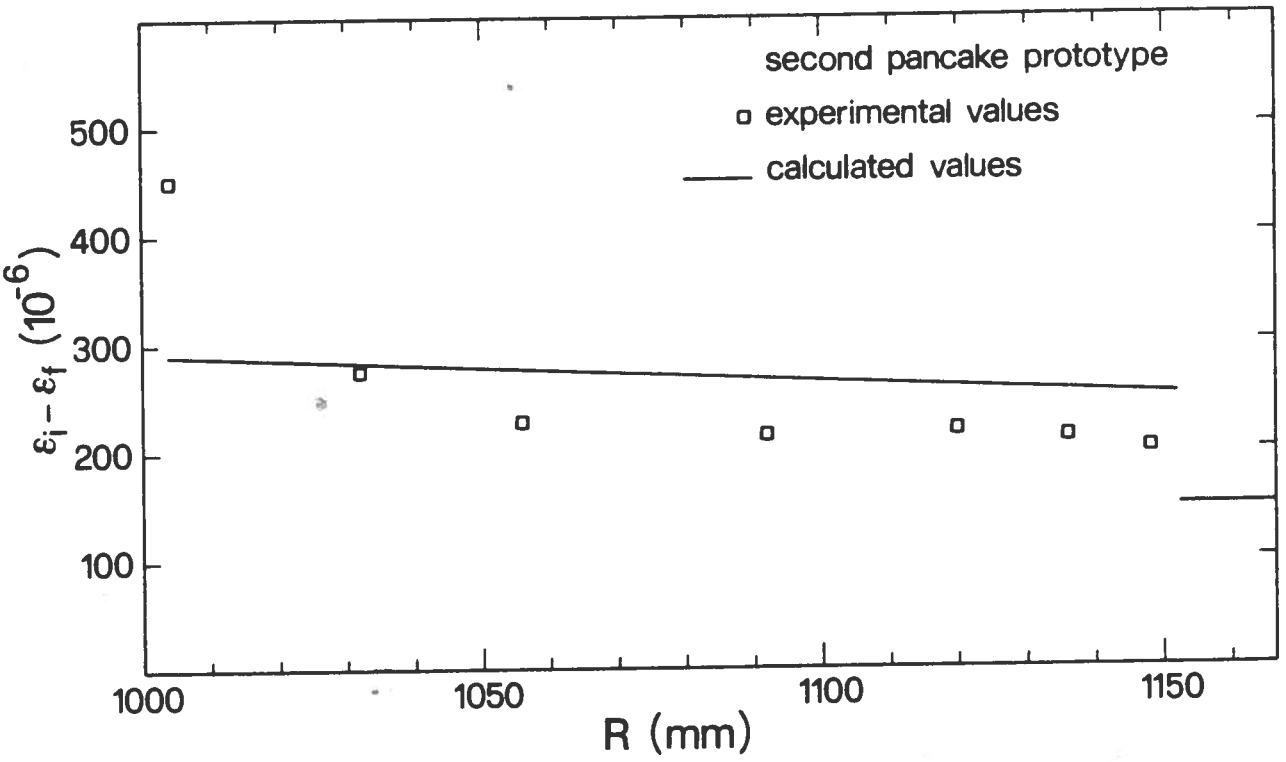

Fig.27 -Tangential strain variation in the second prototype following the mandrel release.

V.2 Inward force tests.

The β sections of the coils, see cap.II and fig.2, have to support an inward radial force when they are negativly excited; even this force are well below the theoritical buckling limit, tests were carried out with the experimental arrangement shown in fig.28.
In the prototypes a lot of G11 radial strips lost tension because of bonding problems (see para IV.2) and so the pancake radial stiffness was lessened; nevertheless coils work in a fully elastic regime and the force level does not affect their performance as it can be deduced from results shown in fig.29.

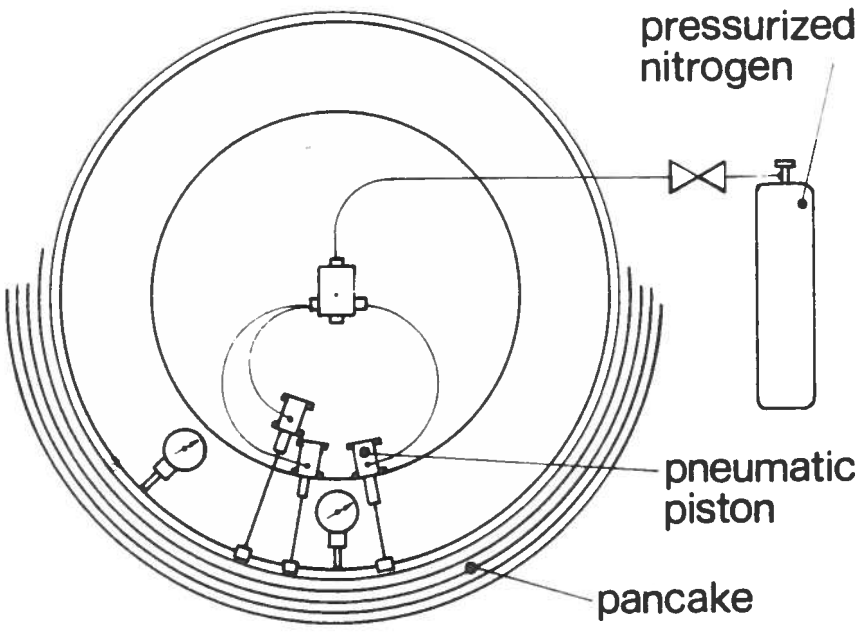

Fig.28- Sketch of the arrangement for the test of inward force. 72
pneumatic piston acted with a force of 550 N for every bar of the pneumatic supply.

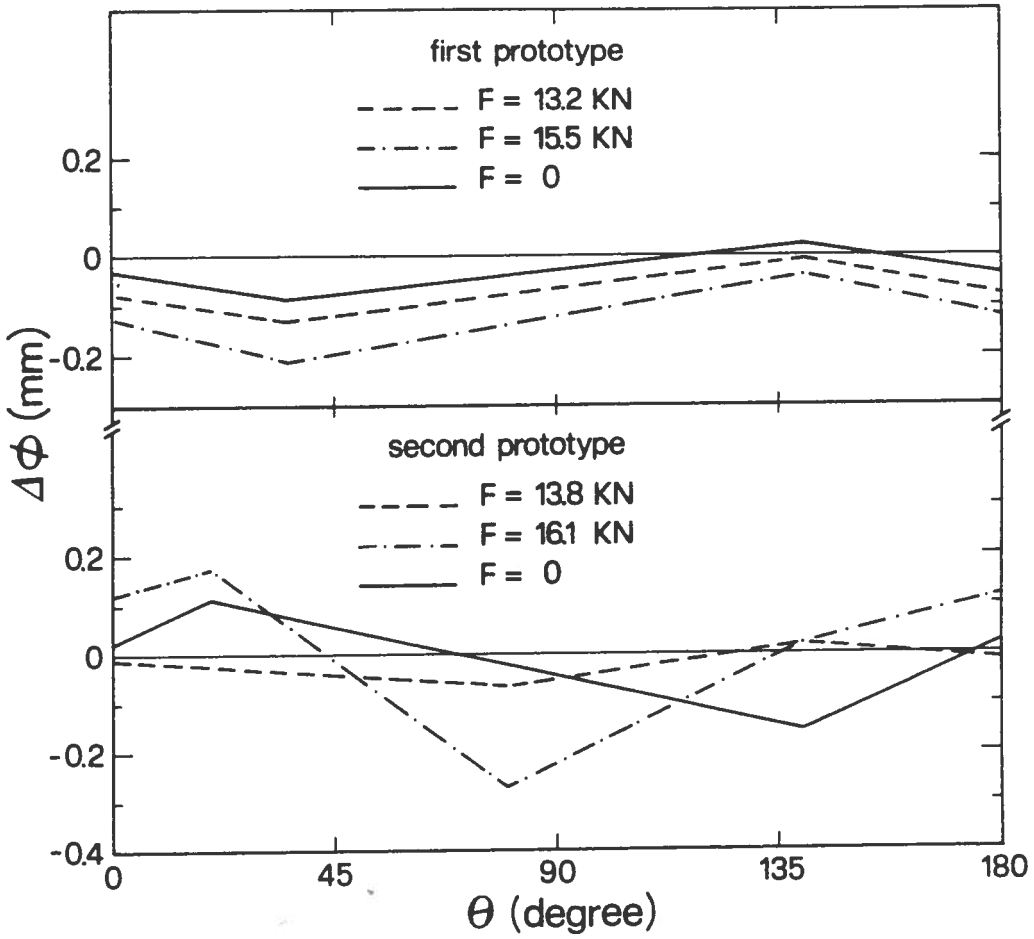

Fig.29- Measured diameter variation due to the action of an inward force. Note that the curve at F=0 refers to release after maximum force was applied. The maximum expected force in the cyclotron is about 10.8 kN.

V.3 Outward force tests

By using the winding mandrel we attempt to check the behaviour of the coil under the action of the large, outward directed, electromagnetic force. Obviously the fields acts on every turn; on the contrary we pushed, by using the mandrel sectors, against the innermost turn and so the resulting stress distribution is a bit different than in the real case.
Nevertheless, by means of this test we was able to check the accuracy of our stress calculation.
In the test condition, the hoop stress distribution is given by:

$$\sigma(r) = P\ (a^2/(b^2-a^2))(1+b^2/r^2)$$

where : $\sigma(r)$ is the hoop stress at radius r

a,b are the internal and external coils radius

P is the radial pressure exerted on the inner turn

By using our geometry we get: $\sigma(a) = 6.63\ P$

$\sigma(b) = 5.64\ P$

We was able to apply a maximum pressure of about 9.4 MPa (total force was 1.4 MN), so checked the pancakes at $\sigma(a) = 62$ MPa and $\sigma(b) = 53$ MPa. In the cyclotron at maximum magnetic field the stress level are near constant in radius and $\sigma \simeq 78$ MPa, see fig.25, and the maximum diameter increase due to this force is expected to be about 1.7 mm.
In fig.30 the test results are plotted and the average diameter increase at different stress level is listed.
Experimental diameter increase is in a quite good agree with that expected one (1.35 mm at 62 MPa raises to 1.7 mm at 78 MPa in the elastic regime) and the very small residual strain after release gives us confidence that cable and insulator will work in elastic regime.

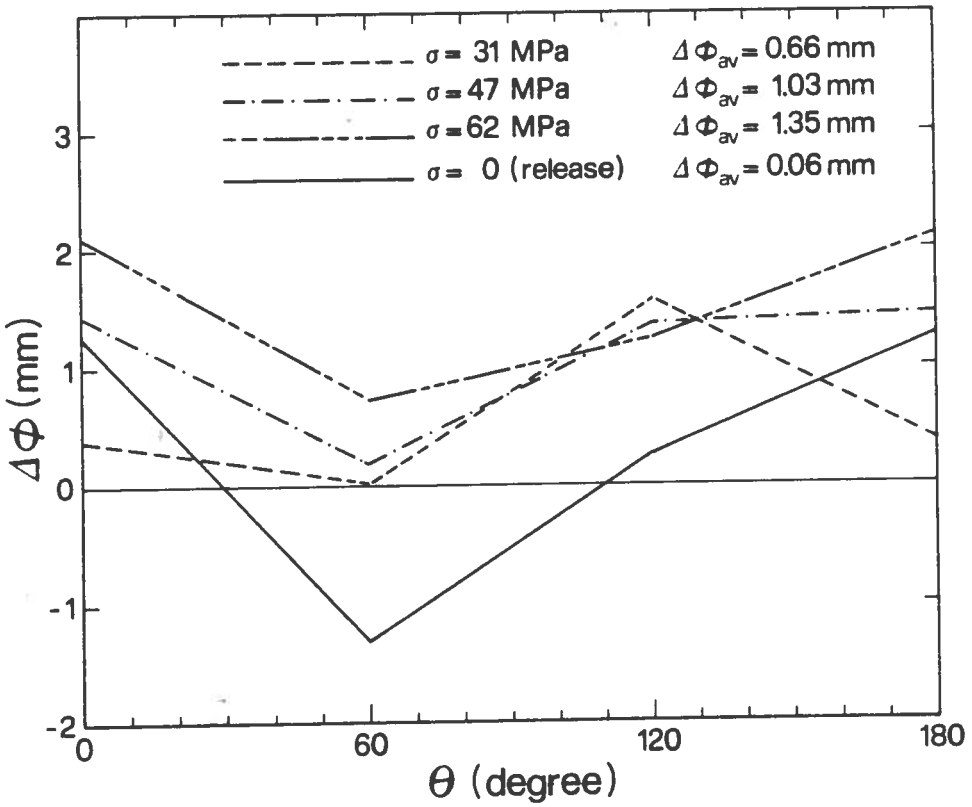

Fig.30 - Diameter increase of the first prototype under the action of an outward pressure. The expected maximum stress during cyclotron operation is about 78 MPa and calculated diameter increase is 1.7 mm. Note that no residual strain remains after pressure release.